NONIMMERSION PULSE-ECHO ACOUSTO-OPTICAL IMAGING NONDESTRUCTIVE TESTING SYSTEM

TRW Systems Group

PREPARED FOR
Army Materials and Mechanics Research Center
March 1973

AMMRC TR-73-10

NONIMMERSION PULSE-ECHO ACOUSTO-OPTICAL IMAGING NONDESTRUCTIVE TESTING SYSTEM

March 1973

N. H. Doshi
R. A. Smith
R. L. Johnson
P. G. Bhuta

Advanced Technology Staff
Space Vehicles Division
TRW Systems Group
One Space Park
Redondo Beach, California 90278

FINAL REPORT - CONTRACT DAAG46-70-C-0103

Sponsored by: Advanced Research Projects Agency, ARPA Order No. 1245

Prepared for

ARMY MATERIALS AND MECHANICS RESEARCH CENTER
Watertown, Massachusetts 02172

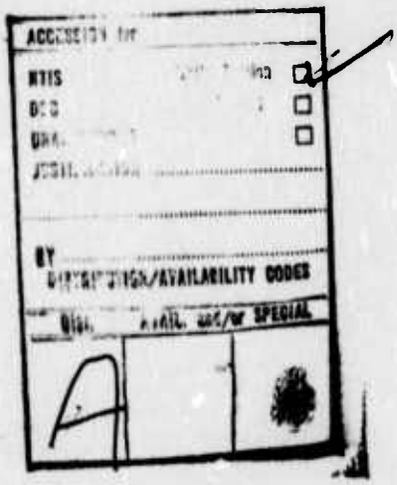

The views and conclusions contained in this document are those of the authors and should not be interpreted as necessarily representing the official policies, either expressed or implied, of the Advanced Research Projects Agency or the U. S. Government.

Mention of any trade names or manufacturers in this report shall not be construed as advertising nor as an official indorsement or approval of such products or companies by the United States Government.

DISPOSITION INSTRUCTIONS

Destroy this report when it is no longer needed.
Do not return it to the originator.

Unclassified

Security Classification

DOCUMENT CONTROL DATA - R & D

(Security classification of title, body of abstract and indexing annotation must be entered when the overall report is classified)

1 ORIGINATING ACTIVITY *(Corporate author)*
TRW Systems Group
One Space Park
Redondo Beach, California 90278

2a. REPORT SECURITY CLASSIFICATION
Unclassified

2b. GROUP

3 REPORT TITLE
NONIMMERSION PULSE-ECHO ACOUSTO-OPTICAL IMAGING NONDESTRUCTIVE TESTING SYSTEM

4 DESCRIPTIVE NOTES *(Type of report and inclusive dates)*
Final Report - June 30, 1970 to 30 March 1973

5 AUTHOR(S) *(First name, middle initial, last name)*
Navin H. Doshi Pravin G. Bhuta
Roy A. Smith
Robert L. Johnson

6 REPORT DATE
March 1973

7a. TOTAL NO. OF PAGES
~~72~~ 73

7b. NO. OF REFS
7

8a. CONTRACT OR GRANT NO.
DAAG46-70-C-0103

b. PROJECT NO
ARPA Order No. 1245

c.

d.

9a. ORIGINATOR'S REPORT NUMBER(S)

9b. OTHER REPORT NO(S) *(Any other numbers that may be assigned this report)*

10 DISTRIBUTION STATEMENT
Approved for public release; distribution unlimited.

11 SUPPLEMENTARY NOTES

12. SPONSORING MILITARY ACTIVITY
Army Materials and Mechanics Research Center, Watertown, Massachusetts 92172

13 ABSTRACT

The technique of Acousto-Optical Imaging (AOI) enables one to "see," on a real-time basis, within optically opaque materials and to detect internal or surface flaws and/or other irregularities which might be present. The process uses an ultrasonic beam to probe the object under study. As it interacts with the object, the ultrasonic beam acquires an acoustical "picture" of the object. Earlier work under the subject contract dealt with imaging of flaws of objects in a transmission mode and required immersion of the object.

This phase of the investigation was devoted to the design and construction of a nonimmersion pulse-echo acousto-optical imaging system. Using the nonimmersion pulse-echo acousto-optical imaging system, images of regular and irregular flaws in specimens were obtained to define the size of the smallest detectable flaw and to measure the accuracy with which depth of flaw can be determined. The report includes a description and operational characteristics of the nonimmersion pulse-echo acousto-optical imaging system.

DD FORM 1 NOV 68 1473

Unclassified

Security Classification

14. KEY WORDS	LINK A		LINK B		LINK C	
	ROLE	WT	ROLE	WT	ROLE	WT
Ultrasonic Frequencies						
Acoustics						
Nondestructive Tests						
Images						
Reflected Sound						
Pulsed Sound						
Nonimmersion Tests						

ARMY MATERIALS AND MECHANICS RESEARCH CENTER

NONIMMERSION PULSE-ECHO ACOUSTO-OPTICAL IMAGING NONDESTRUCTIVE TESTING SYSTEM

ABSTRACT

The technique of Acousto-Optical Imaging (AOI) enables one to "see," on a real-time basis, within optically opaque materials and to detect internal or surface flaws and/or other irregularities which might be present. The process uses an ultrasonic beam to probe the object under study. As it interacts with the object, the ultrasonic beam acquires an acoustical "picture" of the object. Earlier work under the subject contract dealt with imaging of flaws of objects in a transmission mode and required immersion of the object.

This phase of the investigation was devoted to the design and construction of a nonimmersion pulse-echo acousto-optical imaging system. Using the nonimmersion pulse-echo acousto-optical imaging system, images of regular and irregular flaws in specimens were obtained to define the size of the smallest detectable flaw and to measure the accuracy with which depth of flaw can be determined. The report includes a description and operational characteristics of the nonimmersion pulse-echo acousto-optical imaging system.

FOREWORD

The work reported was performed by the Advanced Technology Staff Group of Space Vehicles Division, TRW Systems, Redondo Beach, California. It was sponsored by the Advanced Research Projects Agency (ARPA Order No. 1245). It was performed under Army Materials and Mechanics Research Center Contract No. DAAG46-70-C-0103 with Mr. O. R. Gericke, Chief, Nondestructive Testing Branch, AMMRC, as technical monitor. Mr. N. H. Doshi performed the experiments and designed the acousto-optical imaging system. Dr. R. A. Smith provided consultation and guidance on the design and made key suggestions pertaining to use of cylindrical optics and improvement of signal-to-noise ratio. Dr. R. L. Johnson provided analytical support to the project. Experimental support was provided by Mr. J. W. Wagoner and Mr. C. W. Murrow. Project Manager at TRW Systems was Dr. P. G. Bhuta. The authors wish to thank Mr. O. R. Gericke for his valuable help and suggestions throughout the course of this project. In particular, they want to acknowledge the contribution by Mr. Gericke pertaining to the concept of nonimmersion pulse-echo imaging system configuration.

TABLE OF CONTENTS

		Page
1.0	INTRODUCTION	1
2.0	ACOUSTO-OPTICAL IMAGING APPLIED TO NONDESTRUCTIVE TESTING AND DETERMINATION OF DESIGN CRITERIA	5
	2.1 Review of the Principles of Acousto-Optical Imaging	5
	2.1.1 Sideband Generation and Bragg Condition	5
	2.1.2 Intensity, Demagnification, and Resolution	8
	2.1.3 Nomenclature	8
	2.2 Considerations for Reflected Sound Imaging	10
	2.3 Acoustic Power Transmission and Acoustic Interference	12
	2.3.1 Power Transmission through One Interface	12
	2.3.2 Multiple Interfaces, Plate and Gap	13
	2.4 Implications for Pulse-Echo Imaging	16
3.0	DESIGN ANALYSIS AND SELECTION OF SUBSYSTEMS	18
	3.1 Acoustic Components	18
	3.1.1 Acoustic Transducer	18
	3.1.2 Acoustic Transducer Matching Network	21
	3.1.3 Electrical Power Generator	25
	3.1.4 Determination of Acoustic Power	26
	3.2 Bragg Cell Assembly	29
	3.2.1 Bragg Cell	29
	3.3 Light Source, Optics and Viewing/Recording Equipment	34
	3.3.1 Laser	34
	3.3.2 Optics	35
	3.3.3 Viewing and Recording Equipment	37
4.0	IMAGING OF FLAWS WITH A NONIMMERSION PULSE-ECHO IMAGING SYSTEM	38
	4.1 Preliminary Tests	38
	4.2 Procedure for a Good Nonimmersion Flaw Image	46

TABLE OF CONTENTS (Cont.)

		Page
	4.3 Test Results	47
	4.4 Test Results Analysis	56
5.0	CONCLUSION AND RECOMMENDATION	62
6.0	REFERENCES	65

1.0 INTRODUCTION

Under Contract DAAG46-70-C-0103, TRW has been investigating the pulse-echo method of acousto-optical imaging to determine its applicability to nondestructive testing. This report contains a summary of the work completed under this, the latest phase of the contract. Earlier phases of the contract were devoted to determining the resolution capability of conventional acousto-optical imaging. This work is summarized in earlier reports (Refs. 1, 2, 3).

The specific objectives of the work reported here were (1) perform design analyses for pulse-echo acousto-optical imaging, (2) assemble the necessary equipment, (3) obtain pulse-echo acousto-optical images of specimens containing known flaws, (4) measure the size of the smallest detectable flaw, and (5) measure the accuracy to which depth of flaw can be determined. All of the objectives of the contract were accomplished. The work is reported in detail in the following sections of this report. Before discussing the results, however, a brief explanation of the pulse-echo acousto-optical method and the motivation for this work will be presented.

The advantages of acousto-optical imaging are that it provides images in real time and has relatively simple image processing procedure. With the present system, the optical image can be magnified employing conventional optics and simply projected directly on an observation screen. Improved images can be obtained by using a closed circuit TV system to process the image.

The components required for acousto-optical imaging are relatively simple. One can Bragg image with a CW laser, a high frequency quartz transducer, power oscillator to drive the transducer, plexiglas tank filled with water and several lenses.

The simple acousto-optical imaging scheme, operating in transmission mode, has a limited field of application because of the necessity to immerse the test object. A nonimmersion, pulse-echo imaging system based on the principle of Bragg diffraction would have wider applications.

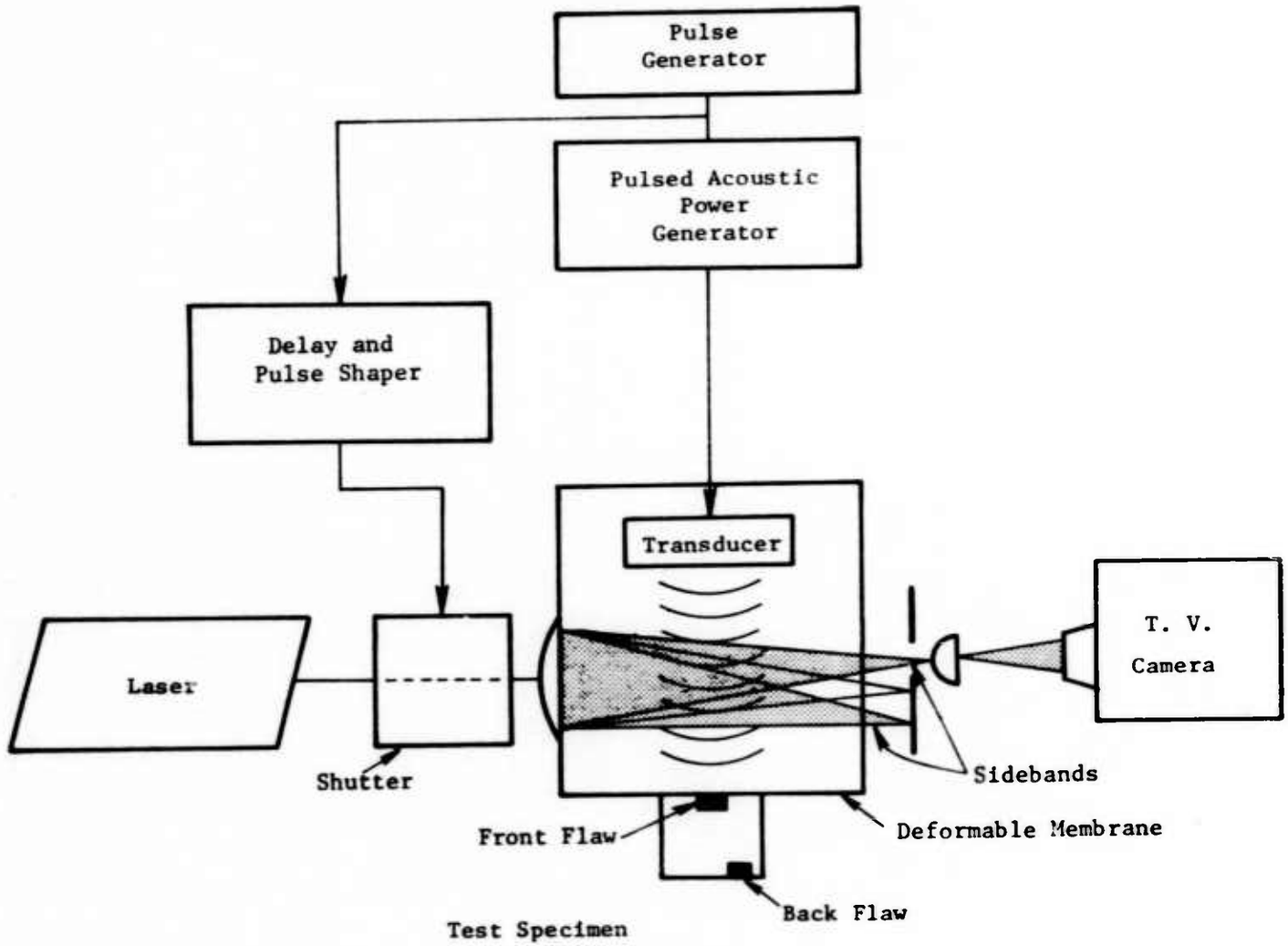

Figure 1.1: Simplified block diagram of a nonimmersion, pulse-echo imaging system.

A brief description of the nonimmersion, pulse-echo system is given as follows (Figure 1.1). The test specimen having flaws is placed in contact with a deformable membrane. The acoustic transducer emits a train of sound pulses at a rate determined by the travel time of the sound in the Bragg cell and the test specimen. A portion of the sound travels through the interface of the membrane and the test specimen. The transmitted sound pulse in the test specimen is reflected by the flaw and enters the light-sound interaction zone. The delay time controlling the laser pulses from the shutter is adjusted so that the laser pulse interacts with the sound reflected from the flaw creating optical sidebands (Bragg diffraction). The first sideband is processed optically to view and record the flaw image. In practice the laser pulse delay is varied until the flaw is located. The depth of the flaw can be deduced from the known delay time and the acoustic velocity in the test material.

A simplified representation of three acousto-optical imaging schemes is shown in Figure 1.2. It is apparent from Figure 1.2 that the nonimmersion pulse-echo imaging system has the following advantages:

1. Allows testing where there is access from only one side. Nonimmersion, pulse-echo imaging needs only one side for flaw imaging.
2. No contact between the test item and the Bragg cell medium.
3. The nonimmersion, pulse-echo imaging system can provide a direct measure of the flaw depth. Neither of the other two system configurations can do this.

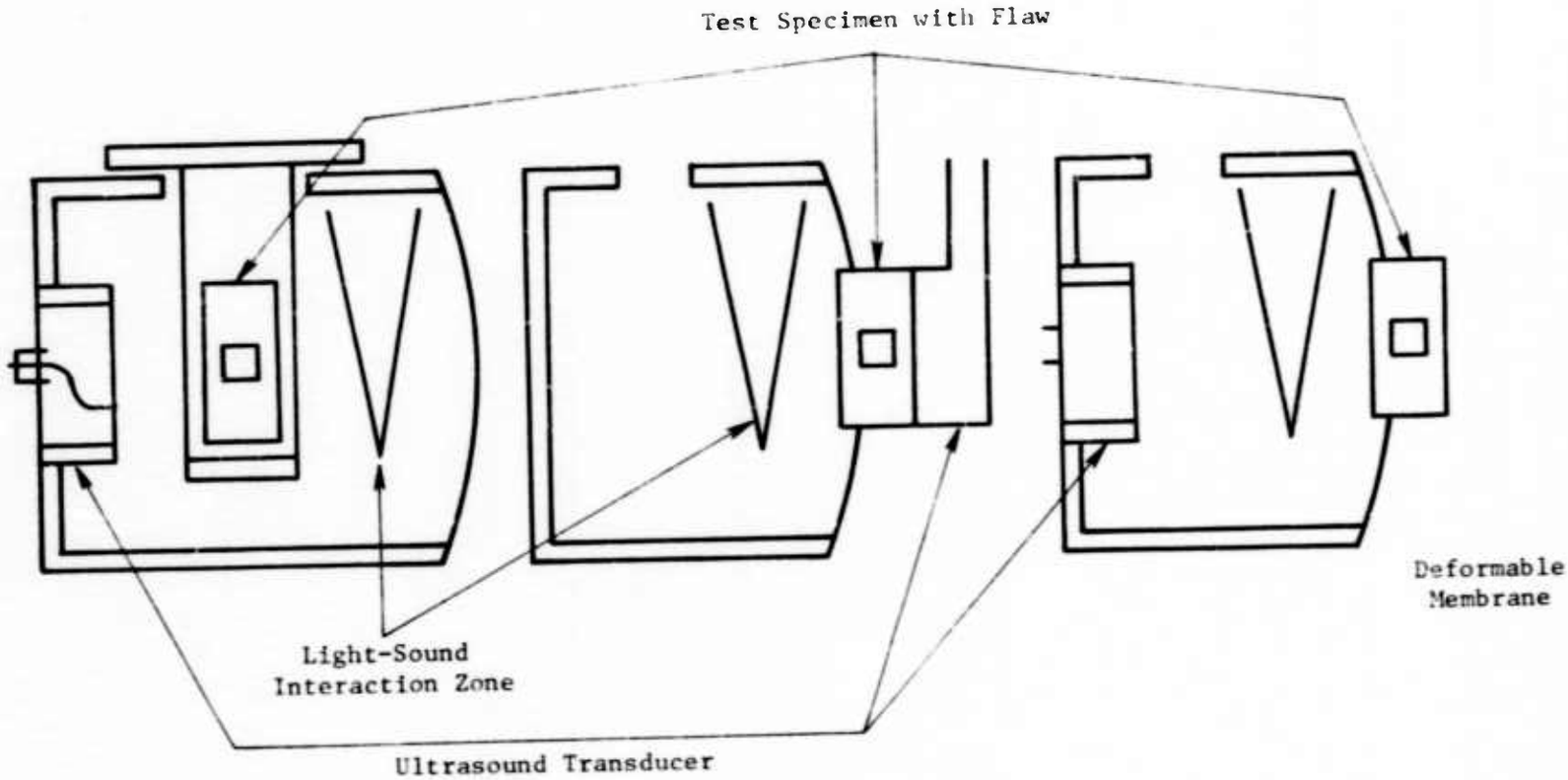

Figure 1.2: Location of transducer, test specimen and light-sound interaction zone in three modes of operation.

2.0 ACOUSTO-OPTICAL IMAGING APPLIED TO NONDESTRUCTIVE TESTING AND DETERMINATION OF DESIGN CRITERIA

In this section a brief review of the physics of light sound interaction is given, with emphasis on application to the pulse-echo method. The reflection and transmission of acoustic energy at interfaces between different materials is reviewed. This leads to several general observations concerning design requirements of the pulse-echo system.

2.1 Review of the Principles of Acousto-Optical Imaging

2.1.1 Sideband Generation and Bragg Condition

Consider an optically transparent tank (Figure 2.1) containing water with a laser light beam parallel to one of the axes of the tank and to the sound wave front (perpendicular to the sound propagation direction). A train of acoustic waves in water generated by the acoustic transducer establishes a cyclic region of compression and rarefaction. This causes the sinusoidal variation of refractive index of water at the acoustic frequency W_s. The resulting volume can be considered a thick phase type hologram. The incoming laser light of frequency W_o reconstructs an image of the ensonified object in light diffracted into directions oriented slightly to either side of the direction of incoming light. Light forming reconstructed images is referred to as sidebands. The sidebands, upon entering the acoustic column, diverge angularly from incoming light which is called the carrier. The angle between the carrier and neighboring sideband images is given by Bragg's law. Bragg's law expresses the condition under which any diffraction grating, such as that produced by acoustic compression and rarefaction, will reflect an incident wave with maximum intensity. The condition of Bragg diffraction is the basis for an alternate view of the acousto-optical imaging system which is the subject of this report. Referring back to Figure 2.1, if an object is placed in the Bragg cell and the acoustic beam is directed on the object, every point of the object is excited (assuming that the acoustic beam covers the entire exposed area of the object). Acoustic waves are reflected from the interior of the object. When these acoustic waves interact with the monochromatic light source satisfying the Bragg condition, an image of the object interior appears at either side of cell illumination light.

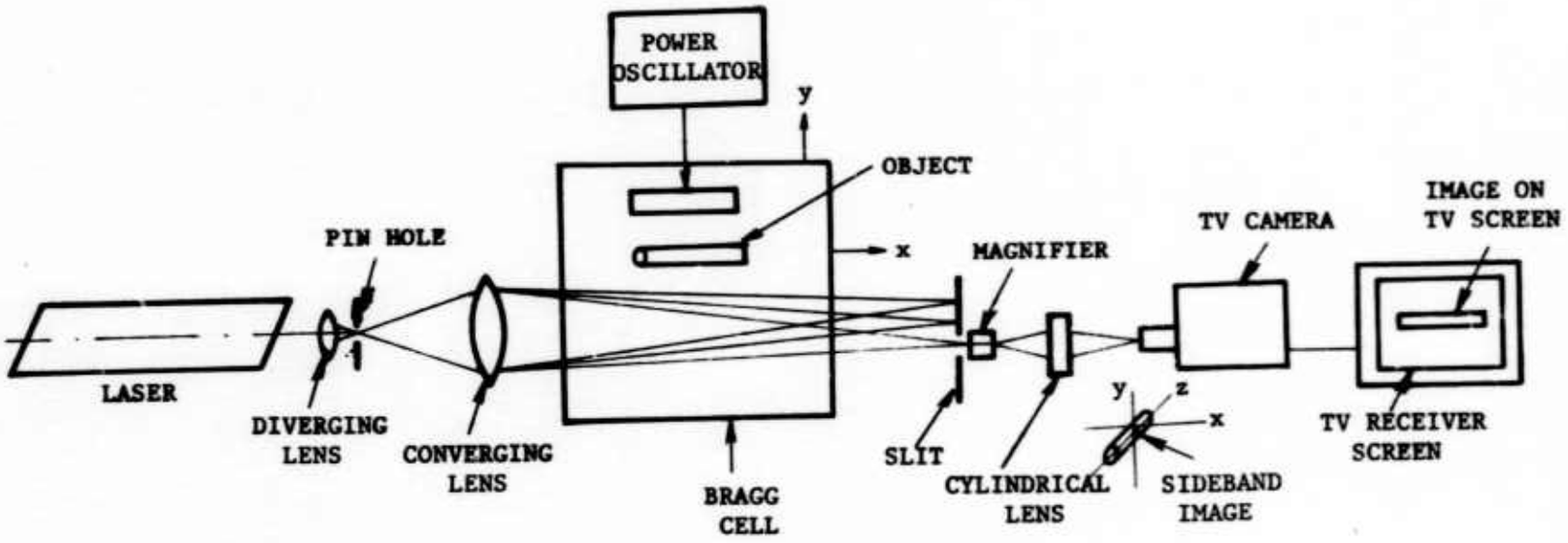

Figure 2.1: System diagram of acousto-optical imaging in transmission mode.

2.1.2 Intensity, Demagnification, and Resolution

The intensity of the first order sideband light I_1 is given by Equation 3 (Table 2.1 (Ref. 4). Note that I_1 is a function of the intensity of laser light I_o, the interaction distance L between the light and sound, the sound intensity P_s and the efficiency of the coupling medium.

Equation 5 (Table 2.1) is an approximation obtained by assuming that the argument of the square of the sine is sufficiently small to replace it by the square of the argument, and the coupling medium is water (Refs. 1, 2, and 3).

As shown in Figure 2.1, a two-dimensional image of the object is visually displayed on a viewing screen. The image of the object undergoes a demagnification, according to Equation 5, only in parallel direction. Note that there is no demagnification in the perpendicular direction. It is an inherent characteristic of Bragg imaging that the resolution limits in the direction of the two orthogonal image axes are independent of each other. The image resolution limit in the horizontal direction (parallel to the laser light) approaches the value of the sound wavelength and in the vertical direction (perpendicular to the laser light) the image resolution approaches three sound wavelengths (Ref. 5).

2.1.3 Nomenclature (Applied to Table 2.1)

c = velocity of light

d = resolution

D = aperture diameter

f = light frequency

F = sound frequency

I_o = light intensity of the laser light beam, watts/cm^2

I_1 = light intensity of the first order diffracted light beam, watts/cm^2

Table 2.1: Equations Applied to Acousto-Optical Imaging

ITEM	DESCRIPTION	EQUATION	FIGURE
1	Bragg diffraction condition for constructive interference	$\sin \alpha = \frac{N\lambda}{2\Lambda}$	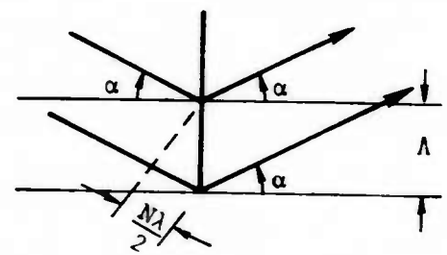
2	Sideband frequencies	$W = W_o \pm NW_s$	
3	Light intensity of first order sideband with a full size image	$\frac{I_1}{I_o} = \frac{\pi^2 P_s (n^2 + 2)(n^2 - 1)}{12 n \rho V^2 L \lambda^2 F \sin \alpha m}$	
4	Simplified form of Equation 3	$\frac{I_1}{I_o} = 1.8\, \ell^2 P_s$	
5	Demagnification of the image	$Q_H = \lambda/\Lambda$ $Q_V = y'/x' = 1$	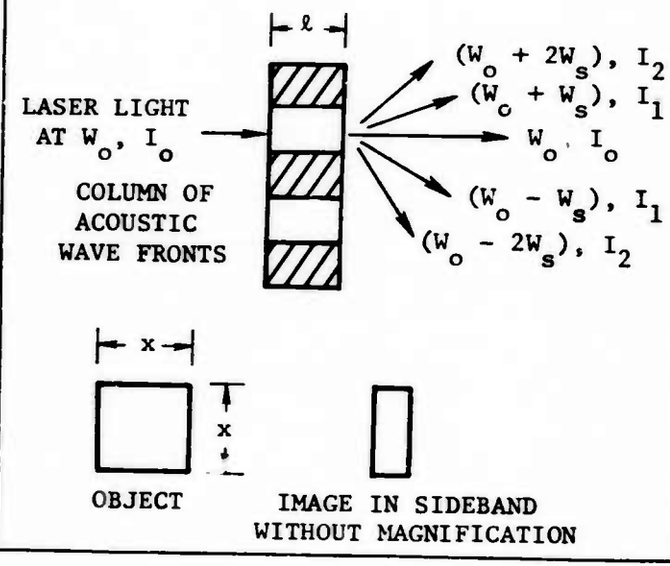
6	Image resolution	$d_H = \frac{\Lambda}{2}$ $d_V = 3\Lambda$; $d_V = \frac{\Lambda}{\phi}$	

Note: For nomenclature and explanation of figures, see Sections 2.1.1 through 2.1.3.

L = length of interaction between sound and the laser light beam measured in the direction of the cylindrical axis, cm

m = modulation index

M = numerical figure of merit referred to water

n = index of refraction

N = order of diffracted light (integer)

= Nth sideband

p = elasto-optic coupling coefficient, $p = 0.31$ for water

P_s = acoustic power density, watts/cm^2

Q = demagnification

R = resistance in ohms

t = thickness of the piezoelectric plate

V = sound velocity, cm/sec

W_o = laser light frequency

W_s = acoustic frequency

ϕ = light cone convergence angle

α = Bragg angle

ρ = density of the Bragg cell medium

λ = wavelength of light

Λ = wavelength of sound

α_m = half the angular width of cylindrically convergent cell illumination light

2.2 Considerations for Reflected Sound Imaging

For pulse-echo imaging, the spectral distribution of the RF pulse train is important. Consider the rectangular wave train (Figure 2.2) of radio frequency f_c, pulse width τ, period T_o and amplitude A applied to the acoustic transducer which generates the acoustic waves in the Bragg cell. Fourier analysis gives the following information about the signal.

- Approximately 90% of the power is contained in the bandwidth $B = 2/\tau$.
- The amplitude of frequency component $f_c = A/2T_o$.
- Each Fourier frequency component is $1/T_o$ H_z apart and total number of frequencies is $n = BT_o = 2T_o$.

The Bragg imaging analysis assumes that the frequency of the sound source is monochromatic. It is apparent that the sound source operated in a pulse mode will not be absolutely monochromatic. Note that the acoustic signal frequency spectrum approaches an impulse function in the frequency domain at f_c as τ/T_o approaches one. Each frequency component of the acoustic wave train Bragg diffracts the light at different angles determined by the ratio of light to sound wavelengths. The net effect of the unwanted frequency components is to blur the image obtained from frequency component f_c.

However, a contradicting requirement is that in reflected sound imaging the accustic pulse should be as short as possible to avoid interaction of two echoes; one from the water-solid interface and another from the flaw which is a solid-air or solid-water interface. This can be explained referring to Figure 2.3. Each reflected acoustic wave transit time is given as follows.

$$\text{Front surface reflected wave:} \quad t_1 = \frac{a + 2b}{V_o} \tag{2.1}$$

$$\text{First flaw reflected wave:} \quad t_2 = \frac{a + 2b}{V_o} + \frac{2d}{V_s} \tag{2.2}$$

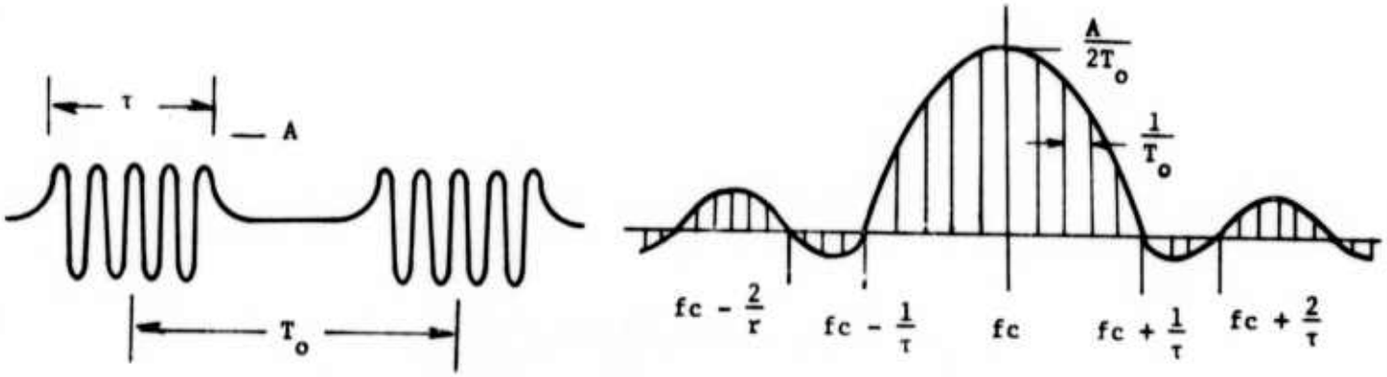

Figure 2.2: Wave train and its frequency spectrum.

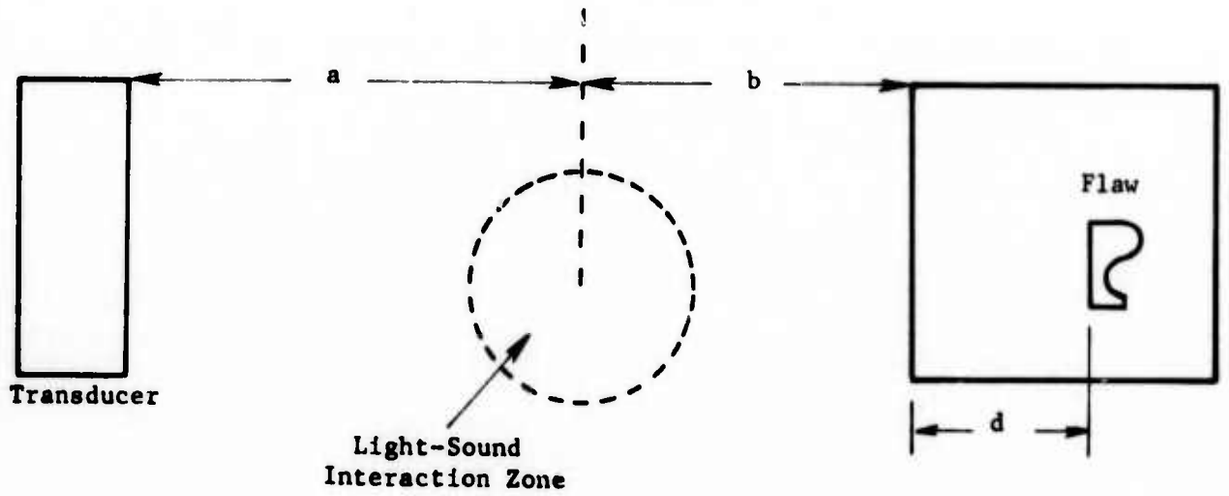

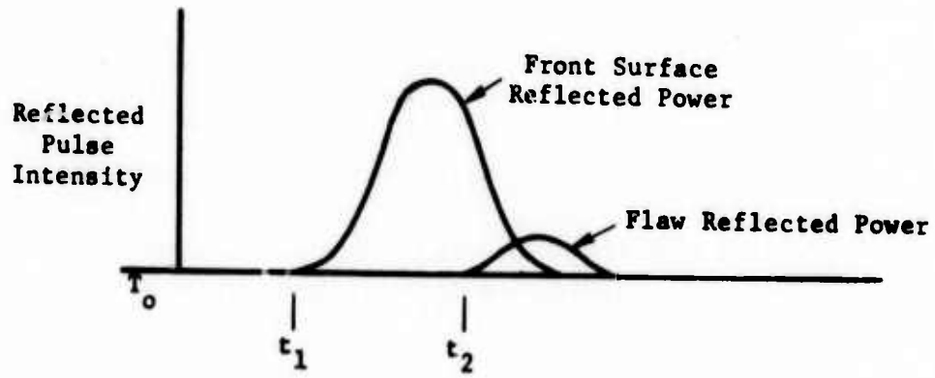

Figure 2.3: Interaction of the reflected sound pulses in a reflected sound AOI scheme.

where V_o is the sound velocity in water and V_s in solid. If the acoustic pulse is wider than $(t_2 - t_1) = 2d/V_s$ microseconds, the tail of the front surface reflected wave will interact with the front flaw reflected wave causing degradation of the image. The closer the first flaw to the front surface, the greater will be the image degradation. To satisfy these two contradicting requirements a compromise is necessary which can be accomplished by the following steps:

1. Reduce T_o based on the system operating characteristics. Reduction of T_o increases the acoustic power of the carrier frequency component f_c and decreases the number of Fourier components n.

2. Shorten the pulse duration so that the two closest echoes do not interfere with each other and at the same time the resolution degradation due to other Fourier components is within limits. The acoustic transducer should be broadband to reproduce the input RF pulse as closely as possible. Note that the wide band transducer has low Q and therefore smaller acoustic power. However, the wide band transducer which reproduces the input with reduced distortion will improve the quality of the image.

Further improvement in reflected sound imaging appears obtainable by use of a Gaussian RF pulse train as input to the power amplifier.

2.3 Acoustic Power Transmission and Acoustic Interference

2.3.1 Power Transmission through One Interface

The acoustic power reflection coefficient α_r and transmission coefficient α_t at normal incidences are given by the following equations:

$$\alpha_r = \left[\frac{\rho_2 C_2 - \rho_1 C_1}{\rho_2 C_2 + \rho_1 C_1}\right]^2 \tag{2.3}$$

$$\alpha_t = \left[\frac{4\rho_2 C_2 \rho_1 C_1}{(\rho_2 C_2 + \rho_1 C_1)^2}\right] \tag{2.4}$$

α_r and α_t are computed for water and selected solid boundaries in Table 2.2. The reflected power density from any flaw in water (Figure 2.3) is α_t times the radiated power density.

Table 2.2: α_r and α_t for Various Boundaries at Normal Incidence for Acoustic Power

Mediums One - Two	Specific Acoustic Impedance $kgm/m^2 - sec \times 10^{-6}$		α_r	α_t
	$\rho_1 C_1$	$\rho_2 C_2$		
Water-Aluminum	1.5	17.0	0.710	0.290
Water-Steel	1.5	46.5	0.885	0.115
Water-Brass	1.5	33	0.830	0.170
Water-Copper	1.5	42	0.865	0.135
Water-Glass	1.5	14	0.665	0.335
Water-Plexiglas or Nylon	1.5	3.2	0.132	0.868
Water-Polystyrene	1.5	2.8	0.091	0.909
Water-Acrylic or Ice	1.5	3.5	0.160	0.840
Water-Hard Metal	1.5	100	0.940	0.060
Water-Mercury	1.5	20	0.740	0.260

2.3.2 Multiple Interfaces, Plate and Gap

The double interface, as in the case of plate and gap, is of interest for the testing of materials (for example, the transmission of sound through a sheet immersed in water, or through a crack in a solid body, or through the membrane of the Bragg cell and the test specimen in contact with the membrane). The wave coming from material A reaches the plate consisting of material B and is split into a transmitted and reflected wave. After passing through the plate, the transmitted wave is split again at the second interface and so forth. The result is a sequence of reflections in both directions inside the plate.

The analysis of the effect of a flaw or double interface on acoustic waves will be discussed with the following assumptions:

1. The interface or a flaw in the test specimen can be considered a disc of air or vacuum having much lower acoustic impedance.
2. The sound wave strikes the interface perpendicular to the interface.
3. The attenuation in the test specimen material is insignificant and remains constant.

The acoustic analysis gives the following expression for the reflectance R and transmittance T:

$$R = \left[\frac{\frac{1}{4}\left(m - \frac{1}{m}\right)^2 \sin^2\left(\frac{2\pi d}{\Lambda}\right)}{1 + \frac{1}{4}\left(m - \frac{1}{m}\right)^2 \sin^2\left(\frac{2\pi d}{\Lambda}\right)} \right]^{1/2} \tag{2.5}$$

$$T = \frac{1}{\left[1 + \frac{1}{4}\left(m - \frac{1}{m}\right)^2 \sin^2\left(\frac{2\pi d}{\Lambda}\right)\right]^{1/2}} \tag{2.6}$$

where $m = \rho_1 C_1 / \rho_2 C_2 = \frac{\text{acoustic impedance of medium 1}}{\text{acoustic impedance of medium 2}}$

d = thickness of the gap

Λ = sound wavelength = C/f

Maxima of T and minima of R occur when $d/\Lambda = 0, 1/2, 1, 3/2$, etc. Maxima of R and minima of T occur when $d/\Lambda = 1/4, 3/4, 5/4$, etc. Our interest lies in very thin gaps and this occurs at first transmittance maximum, i.e., when $d/\Lambda = 0$ to $d/\Lambda = 1/4$. The transmittance T and reflection R for steel and aluminum with air gap are shown in Figure 2.4. Note that the variable F'd (product of frequency in MHz and the gap thickness in millimeters) is plotted on the abscissa.

Assuming that a 10% change in reflected energy is detectable, the product F'd is:

$$F'd \approx 0.7 \times 10^{-7} \text{ for steel}$$

$$= 2 \times 10^{-7} \text{ for aluminum}$$

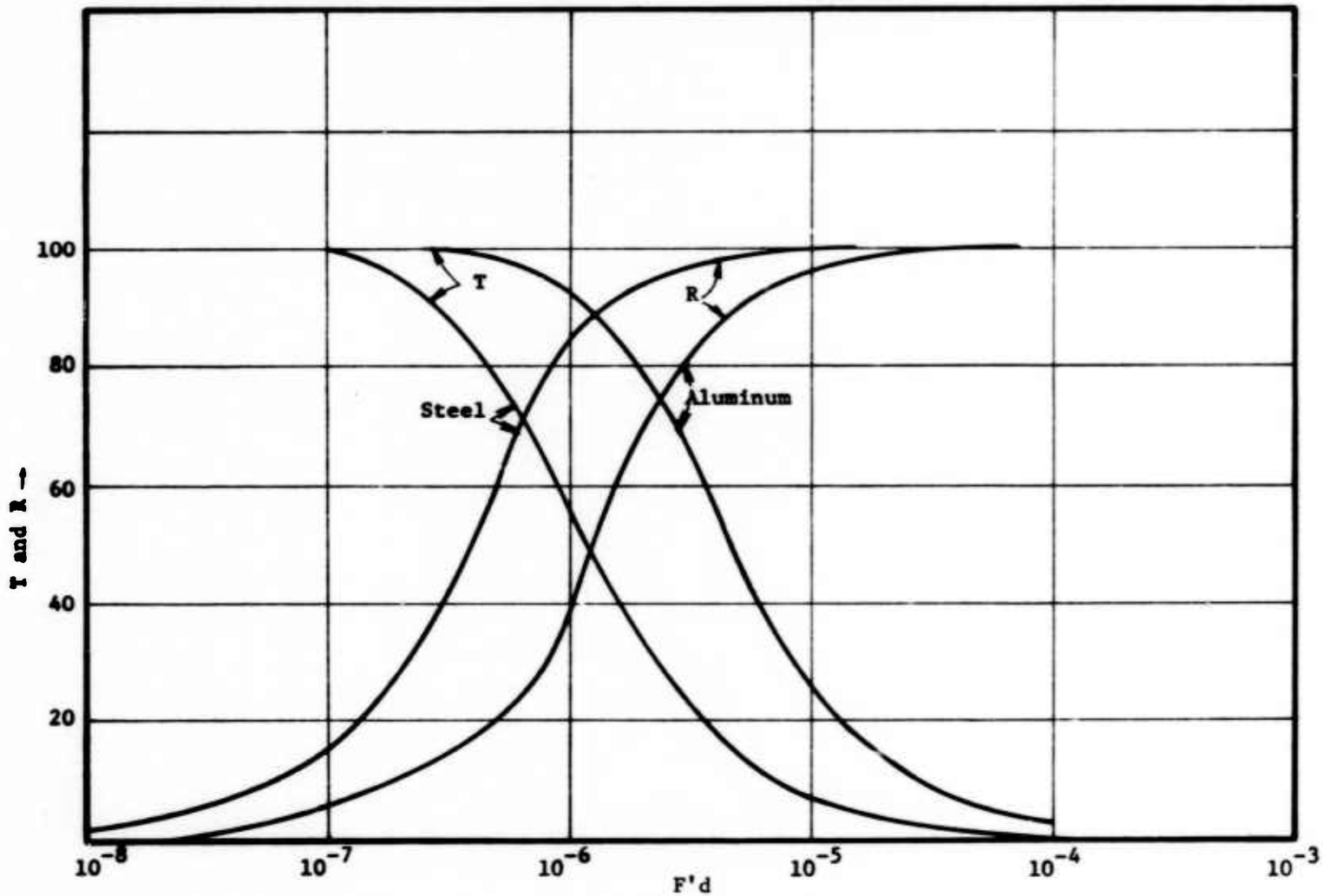

Figure 2.4: Transmittance T and reflection R by air gap in steel and aluminum.
d = thickness of the gap (mm)
f = frequency (MHz)

where F' = acoustic frequency in MHz

d = thickness of the gap in millimeters

For $F' = 10$ MHz

$d = 0.7 \times 10^{-8}$ millimeters (28×10^{-5} microinches)

and $d = 2 \times 10^{-8}$ millimeters (8×10^{-4} microinches)

These computations are hypothetical since in actual practice the reflection is never 100% with an air gap of 10^{-5} mm because of the presence of a foreign layer remaining on the surface even if cleaned most carefully. The effect of the layer is to reduce the reflection and increase the transmission.

2.4 Implications for Pulse-Echo Imaging

The following observations follow from the above analyses and physical considerations:

1. Signal-to-noise ratio*

   The flaw reflected sound intensity in the light-sound interaction zone is a small fraction of the transmitted sound intensity. For example, assuming the acoustic absorption is insignificant, the flaw reflected sound intensity in a light-sound interaction zone for an aluminum test specimen is only 9% of the transmitted sound intensity (Table 2.2). Therefore since the signal strength is proportional to both acoustic and light intensities, these should be as large as practical to obtain a favorable signal-to-noise ratio.

2. Design of a sound pulse train

   The repetition rate and pulse width should be as large as practicable so that the sound source approaches monochromatic. The signal-to-noise ratio also increases with an increase in the

---

* It is the ratio of flaw light intensity to the background light intensity.

repetition rate. The sound pulse width should be such that the front surface echo and flaw echo, or any two adjacent echoes, do not interfere with each other. Shorter sound pulses will, of course have higher flaw depth resolution. The flaw resolution increases with shorter sound wavelength or higher sound frequency.

3. Deformable membrane

The membrane transmitting the sound power from the Bragg cell to the test specimen should be homogeneous and should have no air bubbles which might mask flaws.

3.0 DESIGN ANALYSIS AND SELECTION OF SUBSYSTEMS

The components and subsystems were chosen, designed and assembled based on the design criteria developed previously, past experience and other imposed limitations such as availability, time and cost.

3.1 Acoustic Components

The acoustic components required for pulse-echo imaging are:

- o Acoustic transducer consisting of piezoelectric plate such as x-cut quartz.
- o Matching network to match the impedances of the transducer to that of the generator.
- o The electrical power generator consisting of signal generator and power amplifier.

3.1.1 Acoustic Transducer

The design criteria for the acoustic transducer are that it should have a sufficient bandwidth to reproduce the input pulse with minimum distortion and should be operable in a wide range of frequencies. The selected transducer consisted of quartz piezoelectric crystal mainly because it can be operated from its fundamental resonant frequency to as high as 19th harmonic with reasonable efficiency. The principal advantages of quartz are its mechanical strength and lower internal friction.

The large bandwidth requirement, as discussed in Section 2.0, is mainly to increase the flaw depth resolution.

The transducer bandwidth is determined by the quality factor Q. The mechanical Q of the transducer, Q_m, is given by the following expression:

$$Q_m = n \frac{\pi}{2} \left[\frac{\rho_q V_q}{\rho_w V_w + \rho_b V_b} \right] = \frac{F}{\Delta F} \qquad (3.1)$$

where q refers to quartz

w refers to water

and b refers to the backing material

At fundamental frequency (n = 1) for air and castor oil backing material the Q_m and bandwidth ΔF of a quartz transducer are computed as shown below:

Backing	Loading	Q	ΔF
Air	Water	15.7	95 KHz
Castor Oil	Water	7.85	190 KHz
Air	Quartz	1.5	1 MHz

Table 3.1: Transducer Q factors for various loadings.

The transducer bandwidth can be determined from the step or impulse response of the transducer. This was achieved by applying a very high voltage impulse (less than 0.1 μsec wide) to the radiating transducer and was received by an identical transducer (see Figure 3.1). The measured response to step and impulse excitation is shown in Figure 3.2

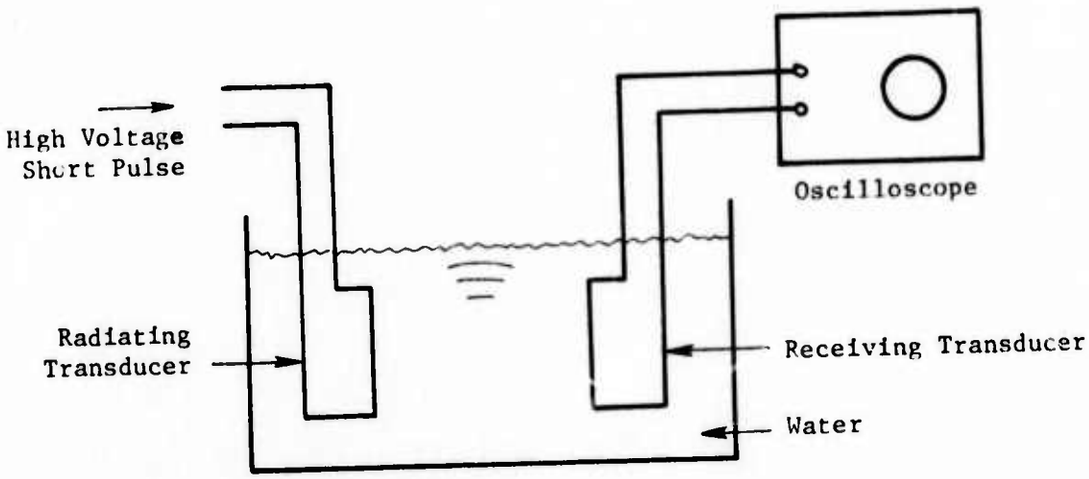

Figure 3.1: Experimental setup to measure the transducer bandwidth.

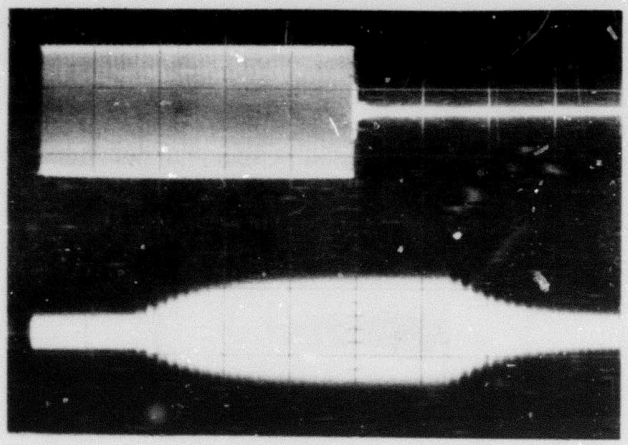

(a) Castor oil backed transducer and receiver. Step response at F = 1.5 MHz. Rise time = 2.6 microseconds. Scale: 1 μsec/cm.

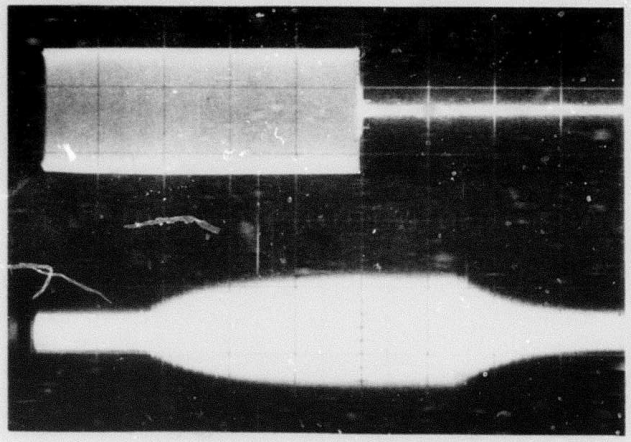

(b) Castor oil backed transducer and receiver. Step response at F = 7.5 MHz. Rise time = 2.6 microseconds. Scale: 1 μsec/cm.

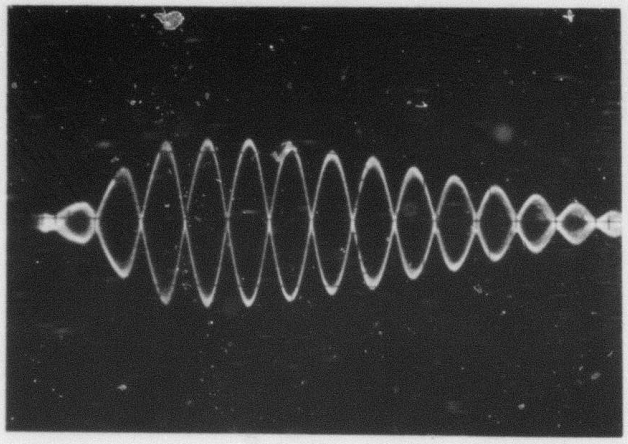

(c) Impulse response of a castor oil backed transducer and receiver. Pulse width $\Delta t = 5.4 \times .5 = 2.7$ μsec. Scale: 0.5 μsec/cm.

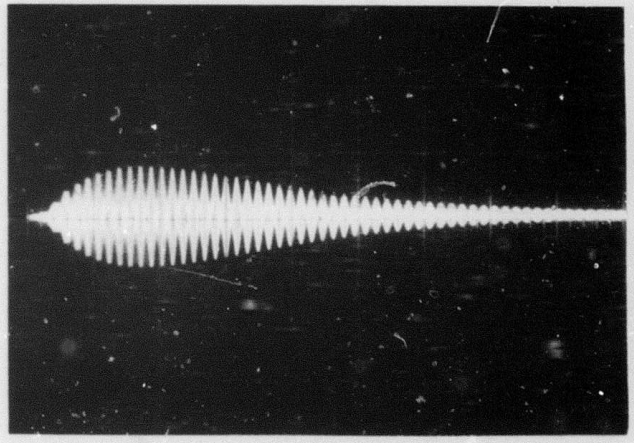

(d) Impulse response of quartz, air backed transducer and receiver. Pulse width $\Delta t = 3.8$ cm x 2 = 7.6 μsec. Scale: 2 μsec/cm.

Figure 3.2; Photographs of the transducer response to a step and impulse input.

for air and castor oil backed transducers. The bandwidth and the pulse width are related as follows:

$$\Delta t \Delta F \approx 1$$

For a castor oil backed transducer, referring to Figure 3.2c: Δt = 2.7 μsec and ΔF = 370 KHz. For air backed transducer, referring to Figure 3.2d: Δt = 7.6 μsec and ΔF = 131 KHz. Note that the step response at 1.5 and 7.5 MHz gives essentially the same value of rise time and therefore the bandwidth (Figure 3.2a,b). The difference between the measured bandwidth and the computed one may be attributed to the mounting losses.

3.1.2 Acoustic Transducer Matching Network

The acoustic transducer is matched to the generator by an LC circuit. To determine the required values of the components of the matching network one needs to determine the transducer radiation resistance R_s and the transducer static capacitance C_o.

An acoustic transducer-generator circuit diagram is shown in Figure 3.3. At half wavelength transducer resonance, the mechanical inductance L_m and capacitance C_m cancel each other out. The electrical capacitance C_1 and inductance L_1 of the matching network are selected so that the resistive component of the impedance looking into the input of the matching network is 50 ohms and reactive component vanishes.

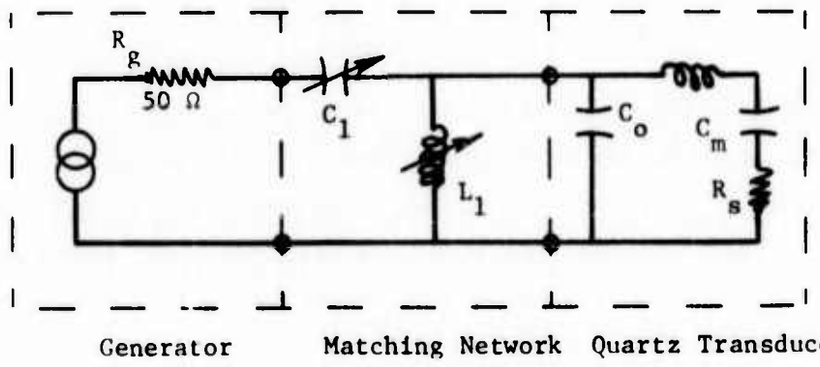

Figure 3.3: Electrical schematic of the generator matching network and the transducer.

The radiation resistance R_s is given by the following equation:

$$R_s = \frac{1}{AF_r^2}\left[\frac{V^2(z_1 + z_2)}{8\,h^2\,\varepsilon^2\,\varepsilon_o^2} + \frac{h^2}{2\pi^2\,(z_1 + z_2)}\right] \qquad (3.2)$$

where A = transducer radiating area

F_r = half wave resonant frequency

V = sound velocity in the crystal = 5760 meter/sec for quartz

z_1, z_2 = acoustic impedance of water and transducer backing

h = piezoelectric constant = 4.9×10^9 volt/meter for quartz piezoelectric crystal

ε = relative dielectric constant = 4.5 for quartz crystal

$\varepsilon_0 = 8.89 \times 10^{-12}$ $\frac{\text{farads}}{\text{meter}}$

For a quartz transducer with air backing, the radiation resistance R_s is:

$$R_s = \frac{1.62 \times 10^{14}}{AF_r^2} \text{ ohms},$$

where F_r is in H_z and A is in $(\text{meter})^2$.

The static capacitance C_o is:

$$C_o = \frac{A\,\varepsilon\,\varepsilon_o}{t} = 40\,\frac{A}{t} \text{ Pico farads}$$

where the quartz plate thickness t is equal to the half wavelength $\Lambda/2$. If the acoustic impedance of the transducer backing medium is other than air, R_s will be proportionally higher. For example, if the castor oil whose acoustic impedance is approximately the same as that of water is used as backing medium, then the radiation resistance at 1.5 MHz and area of 3.9×10^{-3} meters^2 is:

$$R_s = 18{,}461 \times 2 = 36{,}922 \text{ ohms}$$

The values of C_o and R_s for selected transducer configurations are computed and listed in Table 3.2. An estimate of L_1 and C_1 of the matching network (Figure 3.1) is obtained as follows. Assume that the lowest frequency of operation is 4.5 MHz. The corresponding radiation resistance of the castor oil backed transducer is 36,922/9 = 4100 ohms. The matching is obtained if

$$\sqrt{R_g R_s} = \frac{1}{\omega C_1} \quad \text{(Figure 3.3)}$$

and

$$L_1 C_o = \frac{1}{\omega^2} \; ; \; \omega = 3 \times 10^7 \text{ rad/sec}$$

$$(C_1)_{max} = \frac{1}{\omega\sqrt{R_g R_s}} \approx \frac{1}{3 \times 10^7 \sqrt{50 \times 4100}}$$

$$= 75 \text{ Pico farads}$$

$$L_{1_{max}} = \frac{1}{\omega^2 C_o}$$

$$= \frac{10^{12} \times 10^6}{9 \times 10^{14} \times 100} = 11 \text{ micro henries}$$

where minimum C_o which includes the cable capacitance is assumed to be 100 pico farads. An L/C network capable of delivering 100 watts CW power to the transducer was employed. The inductor consisted of a rotary type variable inductor with one terminal open. The range of inductance is 0.04 to 60 micro henries. The range of capacitance of the variable air capacitor is 15 to 353 pico farads.

Table 3.2: Values of R_s and C_o for Quartz Transducers

TYPE OF TRANSDUCER	FUNDAMENTAL RESONANT FREQUENCY MHz	AREA A $(meter)^2$	TRANSDUCER THICKNESS, t (meter)	CAPACITANCE C_o Picofarads	RADIATION RESISTANCE R_s ohms	OPERATING FREQUENCY MHz	OPERATING FREQUENCY Harmonic n
Quartz Water Load Air Backed 2.5" x 2.5" Area	1.5	3.9×10^{-3}	2×10^{-3}	78	18,461	1.5	1
Quartz Water Load	1.5	3.9×10^{-3}	2×10^{-3}	78	36,922	1.5	1
Castor Oil Backed 2.5" x 2.5" Area	1.5	3.9×10^{-3}	2×10^{-3}	78	1,477	7.5	5
"	"	"	"	"	753.5	10.5	7
"	"	"	"	"	456	13.5	9
"	"	"	"	"	305	16.5	11
"	"	"	"	"	218	19.5	13
"	"	"	"	"	164	22.5	15
"	"	"	"	"	128	25.5	17
"	"	"	"	"	67.0	34.5	23
Quartz Water Load Castor Oil Backed An Array of 4 2.5" x 2.5" Transducers	1.5	15.6×10^{-3}	2×10^{-3}	312	369	7.5	5
					114	13.5	9
					76.25	16.5	11
					54.5	19.5	13
Quartz 1.25" x 1.25" Air Backed Water Load	4.0	10^{-3}	0.73×10^{-3}	55	10,000	4	1
Same as above Quartz Load	"	"	"	"	100,000	4	1
					4,000	20	5
					1,235	36	9

3.1.3 Electrical Power Generator

Two power generators were selected since each had different desired capabilities. The pulse power oscillator, Arenberg Ultrasonic Lab Model VI, has the following specifications:

Range of RF frequency:	1 MHz to 100 MHz
Maximum pulse power:	200 watts peak to a 93 ohms load
Minimum pulse width:	4 microseconds
Output impedance:	93 ohms
Maximum pulse repetition rate:	4000 pulses per second

The combination of RF oscillator, pulse generator, diode mixer and wide band amplifiers was also used in place of the Arenberg Model VI. The manufacturer and model number of each component of the subsystem are given below:

RF oscillator:	Hewlett Packard, Model 606AR
Pulse generator:	Hewlett Packard, Model HP202
Mixer:	HP 10514A
Two wide band power amplifiers:	Electronic Navigation Industries, Model 350-L

The specifications of this subsystem are:

Frequency range:	250 KHz to 105 MHz
Amplifier power output:	50 watts to a 50 ohms load
Minimum pulse width:	less than 0.1 microsecond
Delay resolution:	less than 0.2 microsecond

The ENI Model 350-L power generator setup provides a superior characteristic in bandwidth; however, the Arenberg Model VI provides two times the peak power obtainable from two Electronic Navigation Industries Model 350-L operating in parallel.

3.1.4 Determination of Acoustic Power

An analytical expression for acoustic power density P_s or sound intensity at half wave resonance is:

$$P_s = \frac{V^2}{R_s A} \quad \text{for air backed transducer}$$

$$P_s = \frac{V^2}{2R_s A} \quad \text{for water or castor oil backed transducer}$$

where V = applied voltage across the transducer

R_s = equivalent radiation resistance obtained in Table 3.1

A = area of the transducer.

For example, at F = 1.7 MHz, for a quartz/castor oil backed transducer, R_s = 28,745 ohms. Voltage applied across the transducer

$$V = 80 \text{ volts rms}$$

Transducer area = $2.5 \times 2.5 = 6.25 \text{ in}^2$

$$= 40.3 \text{ cm}^2$$

$$P_s = \frac{(80)^2}{28{,}745 \times 40.3} \times \frac{1}{2}$$

$$= 2.76 \text{ milliwatts/cm}^2$$

The sound power density for a castor oil backed quartz transducer at 15.3 MHz (9th harmonic) is determined as follows:

R_s at 15.3 MHz = 355

Applied Voltage V = 30 volts rms

Transducer Area = 40.3 cm^2

$$P_s = \frac{900}{355 \times 40.3} \times \frac{1}{2}$$

$$= 31.45 \text{ milliwatts/cm}^2$$

A cross check was obtained by measuring the sound power employing a calorimeter containing castor oil, a thermistor, and a small heater (Figure 3.4). The calorimeter was exposed to the sound field through a membrane for a period of ninety seconds causing the thermistor resistance change of 40 ohms. Then the electrical power was applied to the heater for a period of 32 seconds to obtain the 40 ohms change in the thermistor resistance. The number of joules to cause the change is:

$$J = \frac{(\text{heater voltage})^2}{\text{heater resistance}} \times \text{time}$$

$$J = \frac{3^2}{47} \times 32$$

$$= 6.12766 \text{ joules}$$

The acoustic power density P_s is

$$P_s = \frac{6.12766}{90\ A_c}$$

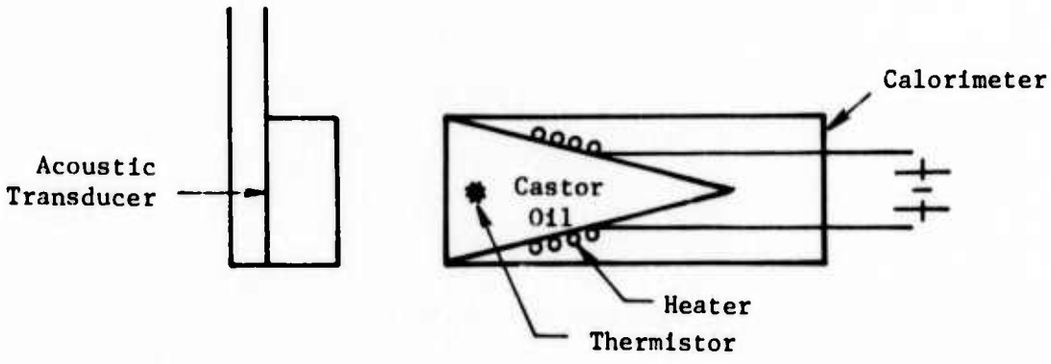

Figure 3.4: Transducer calorimeter setup to measure the acoustic power.

where A_c = area of the calorimeter exposed to the sound field. For $A_c = 1.59$, $P_s = 42.8$ milliwatts/cm^2. The error in the measured value of power density from the computer value is

$$\frac{42.8 - 31.45}{42.8} \times 100 = 26.5\%$$

If there is a matching network between the transducer and the electrical power amplifier, then the power density can be estimated as follows (Figure 3.3):

Normally Rg = 50 ohms

The matching network inductance L_1 and capacitance C_1 are adjusted for the maximum voltage across the transducer at half-wave resonance. Then the acoustic power delivered to the load is:

$$2AP_s = \frac{V_g^2}{50} \eta$$

where V_g is the voltage at the input of the matching network, η is the overall efficiency which includes the efficiency of the matching network and that of the quartz crystal. For a conservative estimate, $\eta = 70\%$.

Then the maximum acoustic power density obtained with the RF power amplifier is:

$$2P_s = 0.7 \times \frac{V_g^2}{50\ A}$$

For the amplifier (Electronic Navigation Industries Model 350-L),

$$V_g = 50 \text{ volts}$$

$$2P_s = \frac{0.7}{2} \times \frac{2500}{50 \times 40.3}$$

$$= 434 \text{ milliwatts/cm}^2$$

Two amplifiers operated in parallel should be able to deliver 868 milliwatts/cm^2 assuming the same overall efficiency. If the Arenberg Model VI is employed, the power density is computed as follows:

$$P_s = \frac{0.7 \times 200}{2 \times 40.3} = 1.73 \text{ watts/cm}^2$$

3.2 Bragg Cell Assembly

The Bragg cell assembly includes the Bragg cell box with the glass windows and the deformable membrane, the water (the acousto-optical interaction medium), the water cleaning system, the Bragg cell position table, and test specimen mounting fixture.

3.2.1 Bragg Cell

The cubic Bragg cell consisted of black anodized aluminum walls with two planes consisting of optical glass and one plane consisting of a deformable membrane. The water level in the Bragg cell was at the 90% mark at atmospheric pressure. The ullage volume in the tank helped avoid rupture in the membrane. The details of the Bragg cell are shown in Figures 3.5 and 3.6. The black color of the Bragg cell walls and the light shields attached to the front glass window will minimize the scattered and reflected light falling on the image plane. One castor oil backed acoustic transducer of size 2.5" x 2.5" having a fundamental resonance of 1.5 MHz was installed permanently on the wall opposite to the membrane. Another similar transducer was installed close to the membrane to minimize the acoustic pulse transit time in the pulse echo imaging mode. Note that the acoustic pulse transit time determines the pulse repetition rate. The width of the light wedge determined by the front optics is 0.75". The transducer for the pulse-echo imaging was approximately 1.50" away from the deformable membrane. Assuming that the maximum thickness of the aluminum test specimen is 4", the one way acoustic pulse transit time t is:

$$t = \frac{1.50}{39.4 \times 1500} + \frac{4}{39.4 \times 6000} = 32 \text{ } \mu\text{sec.}$$

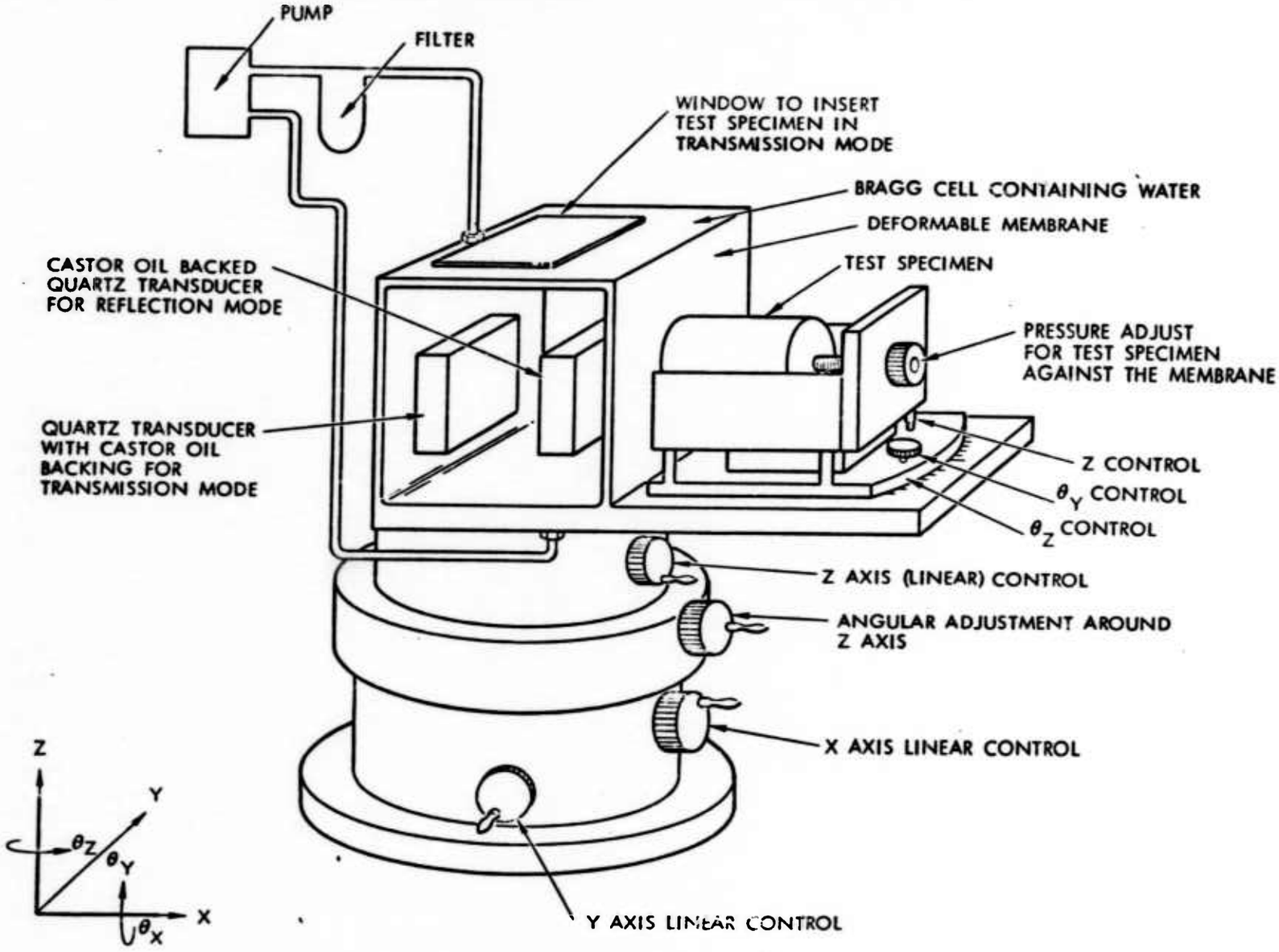

FIGURE 3.5: DETAILS OF BRAGG CELL ASSEMBLY

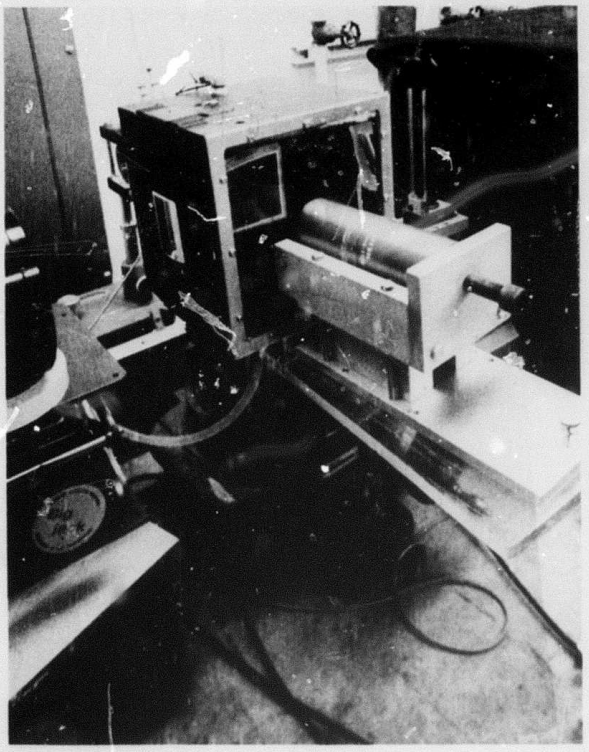

Figure 3.6: Close-up photo of the AOI nonimmersion pulse-echo test setup.

where 1500 meters/sec and 6000 meters/sec are the sound velocities in water and aluminum. The largest pulse repetition rate without ambiguity is 1/2t which comes out to be approximately 15.5 KHz. For most tests, a 2.5" x 2.5" transducer is preferred to the 5" x 5" four quartz plate array (Figure 3.7) since the acoustic power density of the 2.5" x 2.5" transducer is four times greater than that obtained with the 5" x 5" array for the same input power.

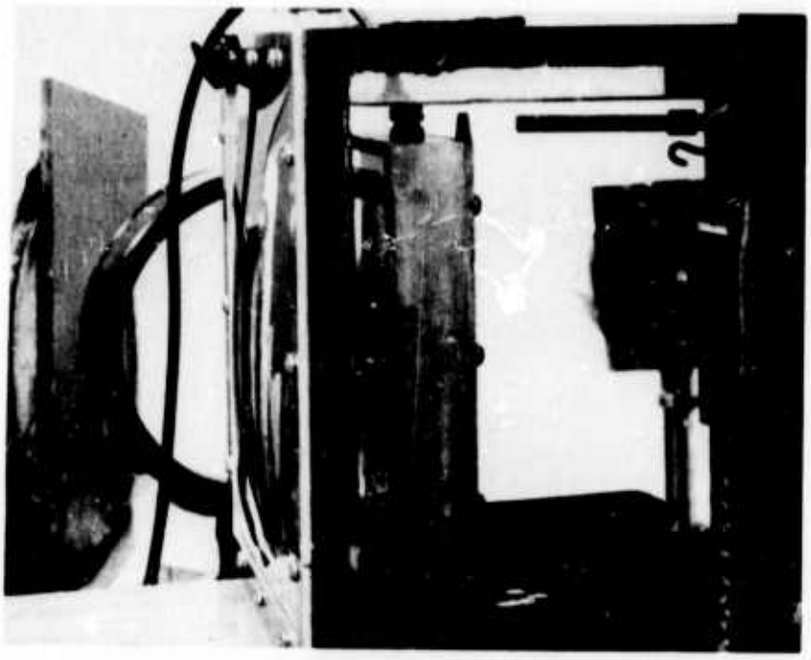

Figure 3.7: Close-up photo of the Bragg cell containing 5" x 5" transducer array.

A large window was provided on the top of the Bragg cell to introduce the test specimen in water so that the AOI system can be operated in the transmission or the reflection mode just by moving the Bragg cell on the y-axis. This flexibility provides an easy method of trouble shooting when the system is operated in a more complex non-immersion reflection mode.

The distilled chlorinated water was constantly cleaned by a water filtering system consisting of a three-micron filter and a pump. The test results indicated that the pump should be kept running for at least four hours before the pulse-echo imaging system is operated.

The selection of the membrane of the Bragg cell was based on the following considerations:

- The membrane material should be strong and plastic so that a sharp corner of a test specimen will not puncture the membrane causing the water leakage. The yielding nature of the membrane should give sufficient time for the operator to either repair

the membrane or remove the water from the Bragg cell. The water leakage is a safety hazard in a high voltage environment and it degrades the precision optical components and mountings.

- o The membrane material should be reasonably deformable so that it can assume the shape of the test specimen area in contact with the membrane.
- o The formation of wrinkles during the membrane installation and testing process should be kept to a minimum since they would be visible on the image plane due to the sound refraction and the air gap between the membrane and the test specimen.
- o It should be available in a thin sheet form and should be homogeneous to minimize the acoustic power absorption.

The following membrane materials were tested:

1. Gum rubber
2. Saran (trade name)
3. Aluminum (0.002" thick)
4. Polyethylene (0.002" thick)
5. Aluminized mylar (0.0006" thick)

Gum rubber and saran were highly absorptive and also not strong enough mechanically. Aluminum membrane worked well except it is not deformable and reacted chemically with water. Polyethylene and aluminized mylar gave acceptable results.

The test specimen surface must be wetted with liquid to avoid the air gap formation between the membrane and the test specimen (Section 2.0). If there is any air gap formation, it will be projected on the image plane, possibly masking a flaw behind the air gap. The wetting liquid can be selected so that the liquid layer provides the acoustic matching between the Bragg cell medium and the solid test specimen. For this reason, glycerine was tried but it did not have a good wetting property. The best results were obtained employing a mixture of water and the Kodak print flattening solution containing ethylene glycol.

The Bragg cell was mounted on a table with an angular adjustment around the vertical axis and linear adjustments along x, y, and z axes. This is useful to achieve the best signal-to-noise ratio by adjusting for optimum Bragg angle and least stray light from the Bragg cell. The best Bragg angle is obtained by adjusting for the largest signal-to-noise ratio. Bragg diffraction is obtained within the band of 3.0 degrees. The adjustment along the transverse and vertical axis (y and z axes) helps to have the center of the object to be imaged, the center of the transducer and the center line of the light beam in one horizontal plane. The bright portion of the light beam gives an improved image compared to that obtained with a weak portion of the beam.

The orientation of the test specimen with respect to the transducer and the light beam is an important factor in Bragg imaging. A v-shaped test specimen mounting fixture was designed and installed with the provision of z, θ_x and θ_z adjustments (Figure 3.5). These adjustments will allow setting the front face of the test specimen in contact with the deformable membrane parallel to the transducer surface and at an appropriate Bragg angle.

3.3 Light Source, Optics and Viewing/Recording Equipment

The required optical components and the light source for Bragg imaging are as follows:

- o CW laser and laser modulator or a pulsed laser
- o Optical components which include beam expander, cylindrical, and spherical lenses, mirrors and slit
- o Viewing and recording equipment

3.3.1 Laser

Two different lasers were employed in the pulse-echo imaging system, the Xenon and the Argon-Ion laser. Xenon laser:

Manufacturer:	TRW Systems
Peak power:	70 to 100 watts

Average power:	10 to 30 milliwatts
Pulse repetition rate:	10 to 100 pulses per second
Pulse width:	1 to 3 microseconds depending on the gas pressure and the applied voltage
Laser wavelength:	514 nanometers

Argon-Ion Laser:

Argon-Ion turnable laser, Spectra Physics Model 165

Maximum CW laser power:	2.0 watts at $\lambda \approx 514$ nanometers
Approximate beam diameter:	1.5 mm
Long term output power stability:	$\pm$ 3%

Acousto-optical light modulator, Zenith Model M-40R

Modulation power required:	1.5 watts RMS around 40 MHz
Modulation bandwidth:	50% at 4.5 MHz
Contrast ratio:	1000 to 1 at low frequencies (DC to 50 KHz)
Maximum light beam diameter:	2 mm
Maximum light beam power:	1 kw/cm^2

Radio frequency oscillator to generate RF pulses for the modulator:
Hewlett Packard 608D

RF pulse power amplifier: Boonton Radio Model 230
Power output: 3 watts to 50 ohms load

Note that the Argon-Ion laser can be operated at the pulse repetition rate of 4000 to 15000 pulses per second limited by the Arenberg power oscillator or the acoustic pulse transit time in the Bragg cell. There is no limitation on the pulse width. However, the useful light pulse width is on the order of the sound pulse width or shorter. Then the range of the light pulse width is from 0.1 to 2.6 microseconds. This will give an average laser power on the order of 20 to 80 milliwatts compared to 10 to 30 milliwatts obtained from the xenon laser.

3.3.2 Optics

The necessary optical components are shown in Figure 3.8. The cylindrical optics are shown over the spherical optics in spite of the

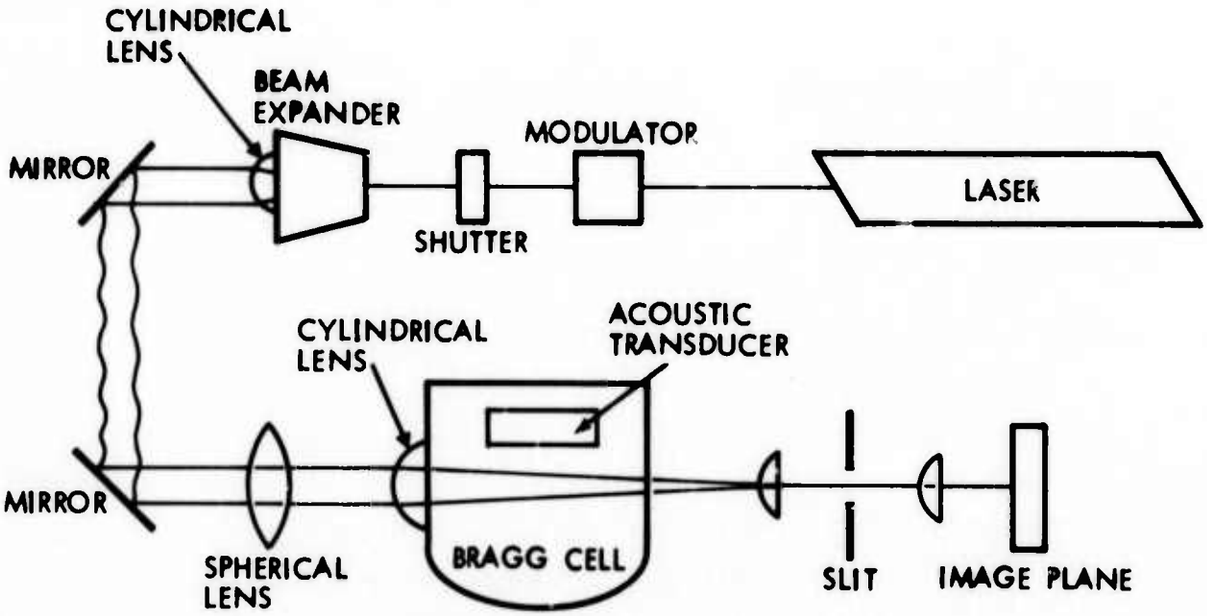

FIGURE 3.8: ARRANGEMENT OF THE LASER AND OPTICAL COMPONENTS IN A PULSE-ECHO IMAGING SYSTEM

fact that the spherical optics had a signal-to-noise ratio two times better than that obtained with cylindrical optics. The important reason to select cylindrical optics over the spherical one is the convenience of operation to minimize the image distortion. The test results indicated that the quality of optical components is an important factor in determining the noise. It appears that the main source of noise is the scattered light from the optical components assuming that the laser output during the off period, as in the case of the xenon laser, is insignificant. The optical components were substituted with those giving the least amount of scattered light on the image plane. A periodical cleaning of the optical component with pure alcohol also helped to improve the signal-to-noise ratio. The dust particles adhere to the optical surfaces due to the static charge; they were removed by a special charge neutralizing brush. The alignment of the optical components in a pulse-echo imaging system is such that there is only one focal plane for the image.

3.3.3 Viewing and Recording Equipment

The image was photographed by exposing the Polaroid film (4" x 5") with the image light. The image can be viewed on a television monitor by replacing the Polaroid film holder with a television camera. The image is required to be demagnified so that it falls entirely on the small area of the TV camera tube. The image can be recorded on a videotape by supplying the TV camera output to a video recorder. The video equipment employed consisted of a Sony 1/2" video recorder Model A-V3600, TV monitor Mode CVM-180UA and the TV camera Model AVC3400.

4.0 IMAGING OF FLAWS WITH A NONIMMERSION PULSE-ECHO IMAGING SYSTEM

The selected and designed components and subsystems were assembled to obtain a nonimmersion pulse-echo imaging system. The individual components and subsystems and the system specifications derived from subsystem/component parameters are listed in Tables 4.1 and 4.2. The photographs and detailed block diagram of the pulse-echo imaging system are given in Figures 4.1 and 4.2. The system is operable in all three modes described in Section 1.0.

4.1 Preliminary Tests

Preliminary tests were conducted in transmission mode to determine the minimum acoustic power density required to image an object. The objects tested were a TRW and T-shaped slots in a 0.01-inch thick brass shim stock. The dimensions of the objects are given in Figure 4.3. The transmission through the brass shim stock at 19.5 MHz is on the order of 10% (Section 2.0).

To determine the primary noise source, the following two tests were conducted. First the CW laser power was reduced gradually from 12 Mw to 1.5 microwatts by introducing the neutral density filters maintaining a constant input power to the acoustic transducer at 10 volts RMS. The transducer boundary and the TRW sign were barely recognizable at the laser power level of 6 microwatts (Figure 4.4). However, the acoustic power density reduction from 100% to 1%, which corresponds to the transducer voltage from 100 volts to 10 volts, degraded the image substantially (Figure 4.5). A recognizable image of the "TRW" sign was obtained with a minimum transducer voltage of 5 volts. Note that these tests were conducted with cylindrical optics. The substitution of these lenses with inferior quality lenses degraded the image substantially. The minimum transducer voltage required employing spherical optics was on the order of 3 volts. It was concluded from these test results that the primary sources of the scattered light on the image plane were optical components.

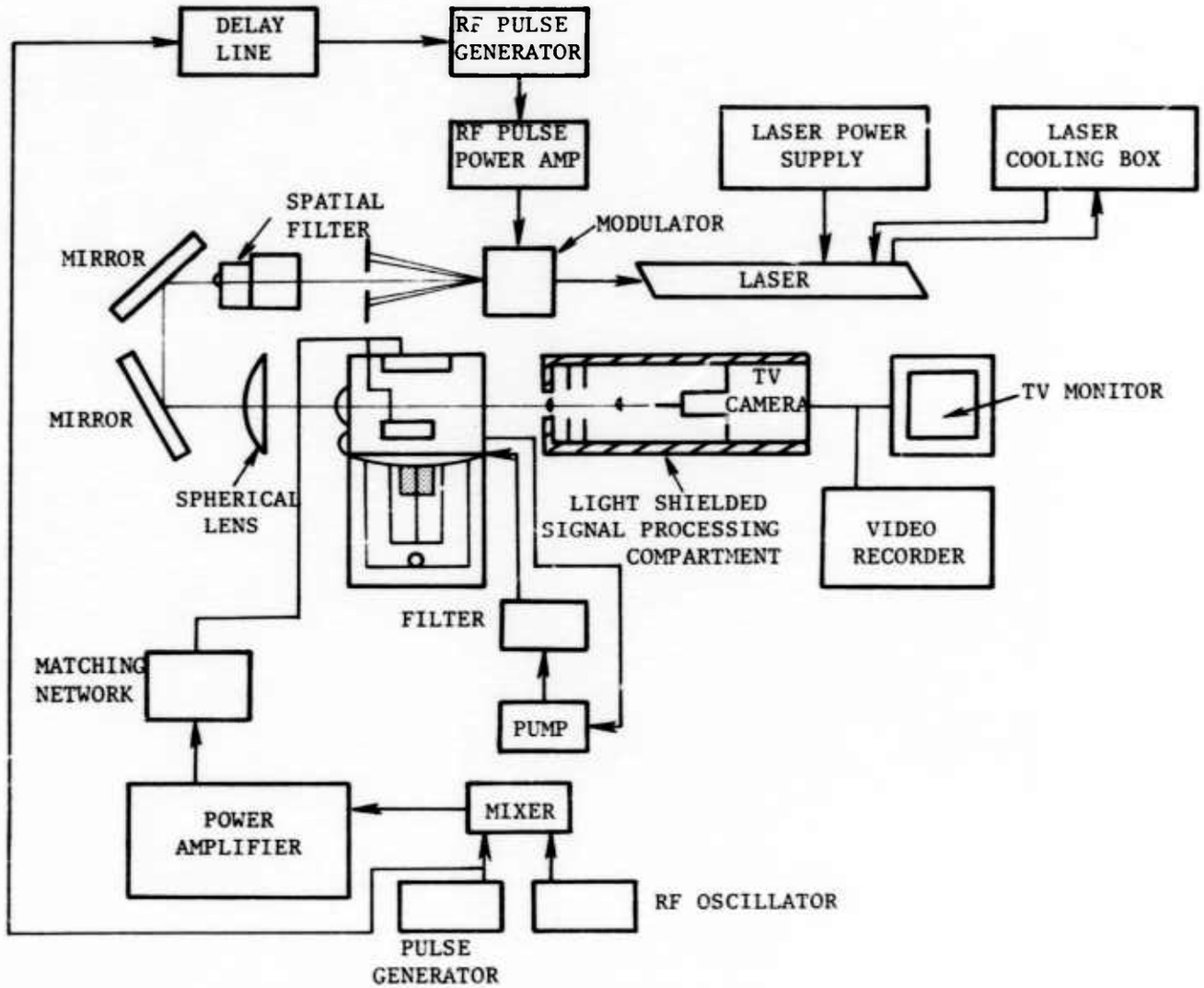

Figure 4.1: Detailed system block diagram of the nonimmersion pulse-echo AOI system.

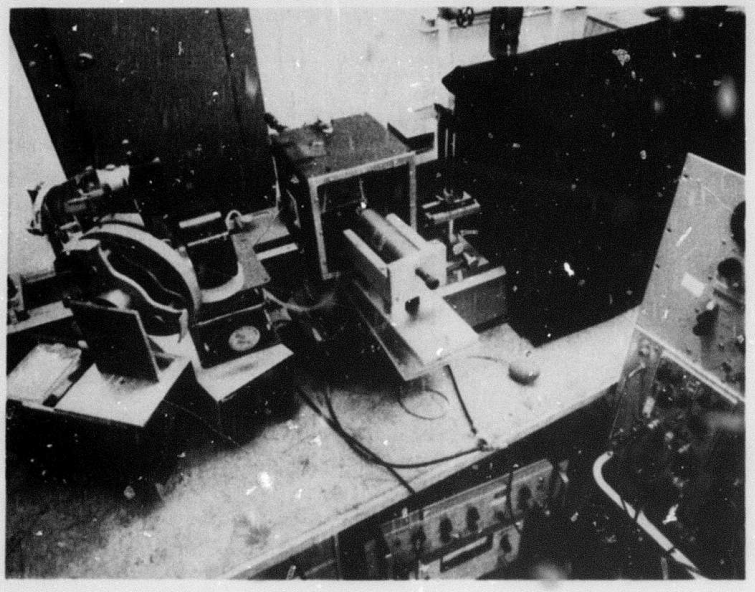

Figure 4.2: Photograph of pulse-echo imaging system.

Table 4.1: List of Components and Subsystems Employed in a Nonimmersion Pulse-Echo Imaging System

1. Laser: CW Argon-ion tunable laser, Spectra Physics 165

2. Acousto-Optical Modulator: Zenith M-40R

3. Modulator Driver: RF pulse generator, Hewlett-Packed 608D
   RF pulse amplifier, Boonton Radio 230

4. Transducer RF Power Source: Arenberg Ultrasonic Lab. VI
   or RF oscillator, Hewlett Packard 606AR
   pulse generator, Hewlett Packard 202
   mixer, Hewlett Packard 10514A
   wideband RF amplifier, Electronic Navigation Industries, 350-2

6. Variable Laser Pulse Delay Generator: Hewlett-Packard 202

7. Oscilloscope: Tektronix Model RM35A

8. Viewing and Recording Equipment: Sony 1/2-inch equipment consisting of recorder model A-V3600, TV monitor model CVM-180UA and TV camera model AVC3400

9. Optics: Cylindrical optics distributed by Rolyn

10. Bragg Cell Assembly: TRW fabricated Bragg cell assembly

11. Acoustic Transducer: TRW fabricated transducer consisting of x-cut quartz plate

Table 4.2: System Specifications

Laser Power:	0.1-2.0 watts CW at 514 Nanometer wavelength
Laser Modulation Output Power:	0.05 to 1 watt peak
Laser Pulse Repetition* Rate:	DC to 15,000 pulses/second, limited by acoustic pulse transit time
Acoustic Power Density at the Transducer Face:	1.73 watts/cm^2 max for a 2.5" x 2.5" transducer and 0.43 watts/cm^2 max for 5" x 5" transducer array
Usable Acoustic Frequency:	1.7, 5.1, 8.5, 11.9, 15.3, 22.1, 25.5, 28.9, 32.3 and 35.9 MHz
Transducer Bandwidth:	370 kilohertz
Electrical Power to the Transducer:	0-100 watts employing two ENI 350 power amplifiers in parallel. 0-200 watts peak employing Arenberg power oscillator, Model VI, having a minimum acoustic pulse width of 3 microseconds.
Equivalent Acoustic Noise Power Density:	120 milliwatts/cm^2
Detectable Flaw Depth at 15.3 MHz and 200 watts Peak Power:	0.125 to 3.5" for aluminum
Estimate of Image Resolution:	0.12 inch at 5 MHz 0.06 inch at 10 MHz 0.03 inch at 20 MHz
Estimate of Flaw Depth Resolution:	0.125 inch

---

* DC to 4,000 pulses/second, if Arenberg power oscillator is used.
DC to 15,000 pulses/second, if ENI amplifiers are used.

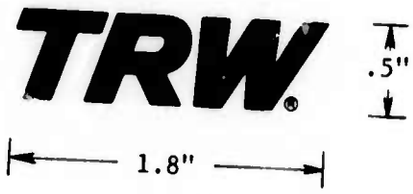

(a)

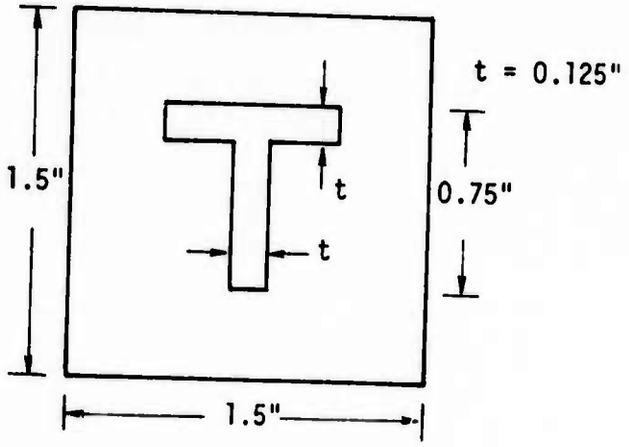

(b)

Figure 4.3: Dimensions of the TRW and T signs in a 0.010" thick shim stock.

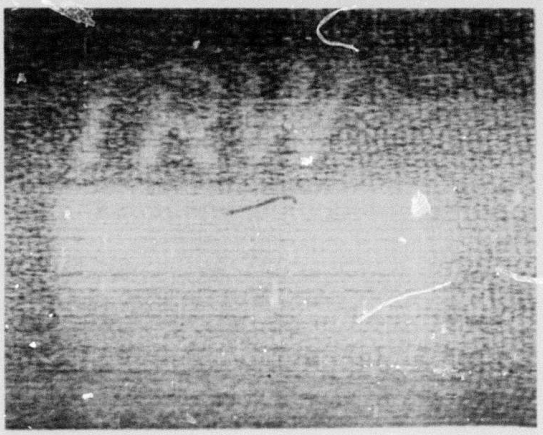

(a) Laser power: 12 milliwatts
Photo exposure time: 0.5 second

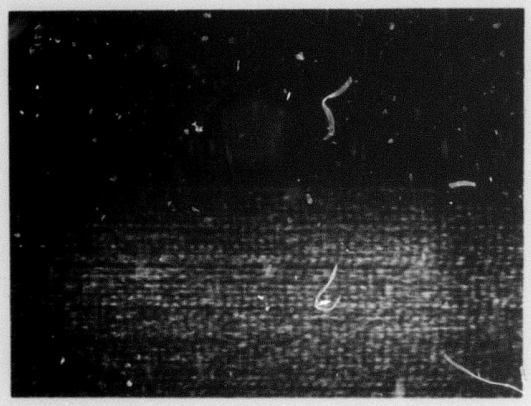

(b) Laser power: 48 microwatts
Photo exposure time: 1.5 min

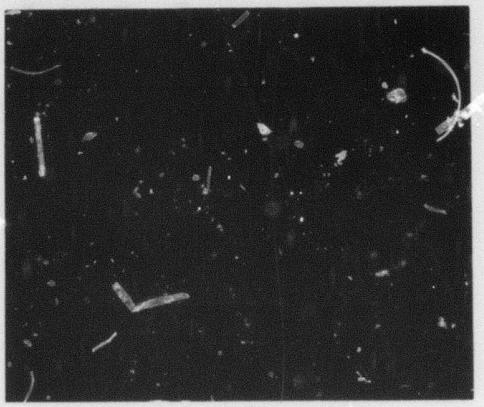

(c) Laser power: 6 microwatts
Photo exposure time: 5 minutes

Figure 4.4: Images of TRW sign in transmission mode with decreasing laser light.
Test Conditions: Acoustic Frequency: 19.5 MHz
Transducer Voltage: 10 volts

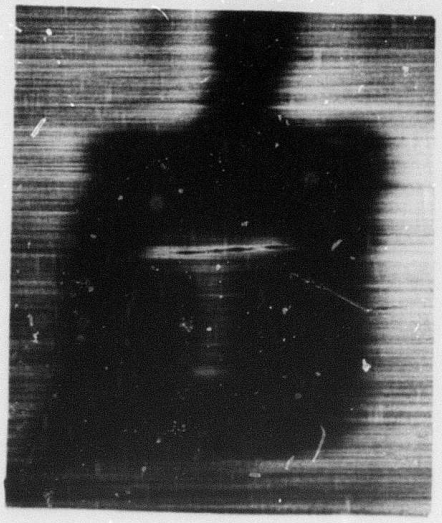

(a) Transducer voltage: 100 volts
Photo exposure time: 1/50 second

(b) Transducer voltage: 25 volts
Photo exposure time: 1/5 second

(c) Transducer voltage: 10 volts
Photo exposure time: 1 second

Figure 4.5: Images of "T" sign in transmission mode with decreasing sound power.
Test conditions: Laser power: 12 Mwatts
Acoustic frequency: 19.5 MHz

4.2 Procedure for a Good Nonimmersion Flaw Image

Based on the test results the following procedure was developed to obtain a good flaw image:

a. Run the Bragg cell water cleaning system for several hours before the start of the imaging.

b. Make sure that every optical component surface is reasonably clean.

c. Make sure that the central portion of the beam (bright part) falls on the front surface of the Bragg cell.

d. The optical alignment of the optical components preceding the Bragg cell should be such that the main beam line on the image plane is of uniform thickness and with minimum distortion.

e. Adjust the RF frequency of the oscillator driving the transducer amplifier for the brightest transducer image. The transducer image is obtained either in a CW mode or in a pulse mode. Then, change the Bragg cell angle to avoid the transducer image. This will insure that the multiple reflections between the diaphragm and the transducers will not create sidebands and therefore will not mask the flaw image.

f. Mount the test specimen so that the front surface of the test specimen is in contact with the membrane. The surface is required to be wetted with the wetting solution so that there are no air bubbles between the membrane and the test specimen front surface. Apply enough pressure so that the operator sees the wetting solution squeezed out of the junction of the membrane and the test specimen.

g. Set the angle of the test specimen by adjusting the angle of the test specimen mounting fixture to obtain the brightest test specimen front surface image. This requires the correct setting of the delay time of the laser pulse determined from the calibration.

h. The image quality is improved further by adjusting the following controls:

- o focusing of the image
- o transducer frequency
- o Bragg angle
- o the pulse delay time and pulse width, and
- o TV monitor controls

The flaw image is obtained by increasing the delay time so that the sound wave front reflected from the flaw interacts with the properly delayed light pulse. The sound pulse width, as discussed previously, determines the brightness and the flaw depth resolution. The laser pulse delay time determines the depth of the flaw from the front surface.

4.3 Test Results

Tests were conducted employing the systems described in Section 4.1 and test specimens with known flaws. The test specimens consisted of aluminum round bar of 2.0" diameter and thicknesses ranging from 0.25" to 3.0". The back surface of each test specimen had recessed flaws of triangular, square, circular and trapezoidal shapes. The details of each test specimen are given in Table 4.3 (see Figure 4.6).

The system was set up in an immersion-reflection mode employing test specimen part No. A-1/2-4T. The details of the test conditions and the image are shown in Figure 4.7. The transducer voltage was reduced so that the image of the flaws was just barely visible. The minimum transducer voltage was on the order of 33 volts RMS compared to 10 volts RMS obtained earlier. This appears to be due to the power loss in the reflection mode and the modulator noise. The acoustic noise power density is then on the order of 120 mwatts/cm^2 compared to 12.0 mwatts/cm^2 obtained previously in a CW transmission mode.

The test specimen part No. A-1/2-4T was then tested in the reflection mode following essentially the procedure described in Section 4.2. The photographs of the flaw images are shown in Figure 4.8. Note that the unfilled holes and the membrane form acoustic lenses causing strong

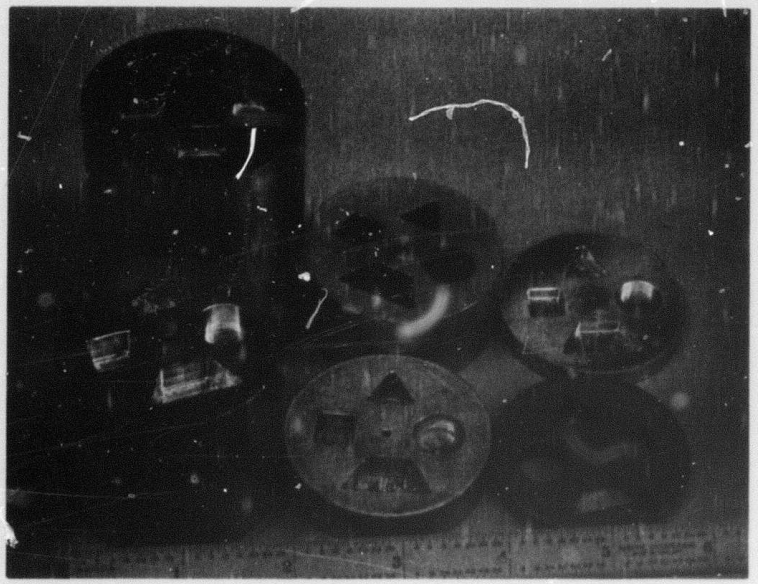

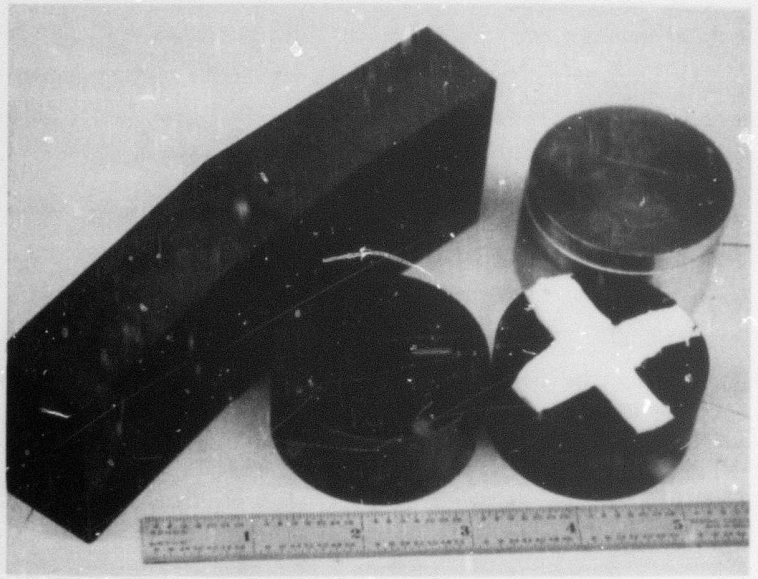

Figure 4.6: Photographs of test specimens of known flaws employed in the pulse-echo imaging system.

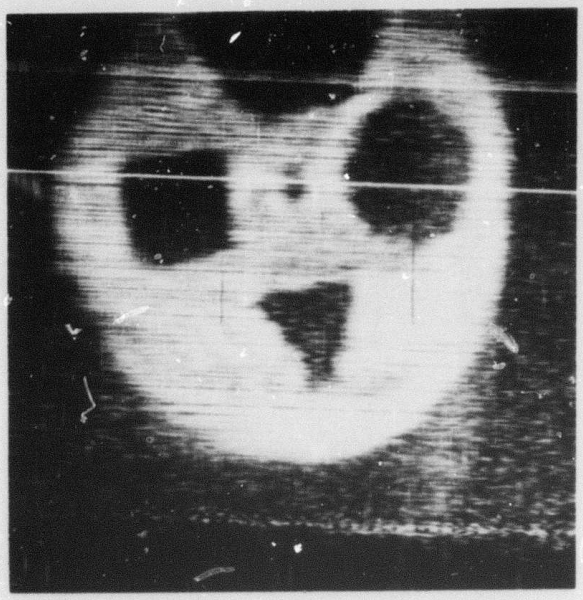

Figure 4.7: Image of test specimen part No. A-1/2-4T in immersion-reflection mode.
Test conditions: Acoustic frequency: 18.7 MHz
Transducer voltage: 100 volts RMS

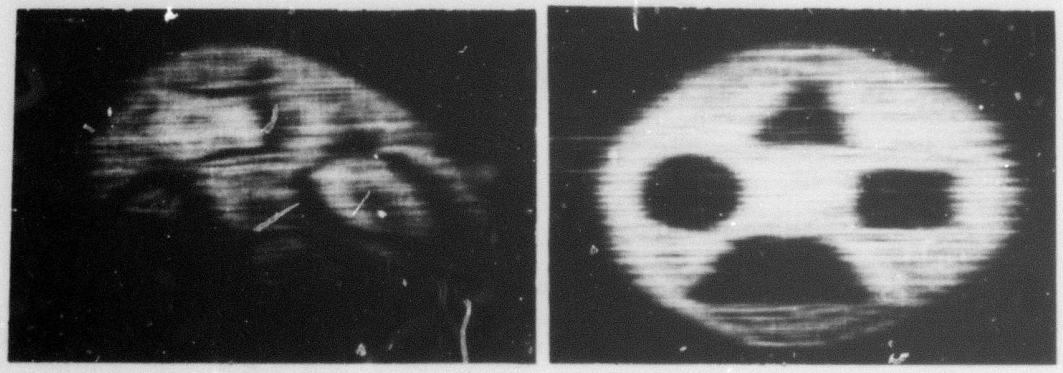

(a) Acoustic frequency: 15 MHz
Part No. A-1/2-4T
No.ρC rubber plugs

(b) Image with ρC rubber plugs. Test conditions are the same as in (a).

Figure 4.8: Images of the test specimen part No. A-1/2-4T in nonimmersion pulse-echo mode.

Figure 4.9: Image of the test specimen part No. A-1/2-4TA in nonimmersion pulse-echo mode at 36 MHz.

Table 4.3: Details of the Test Specimen in the Nonimmersion Pulse-Echo Acousto-Optical Imaging System.

ITEM	TEST SPECIMEN PART NO.	TEST SPECIMEN MATERIAL	DESCRIPTION OF THE TEST SPECIMEN	FIGURE NO.
1	A-1/2-4T	Aluminum	Triangular, square, circular and trapezoidal through holes in a 0.5" thick aluminum plate.	4-8
2	A-1/2-4TA	Aluminum	Same as above with the holes plugged with ρC rubber.	4-8
3	A-1/4-4R	Aluminum	Same as item 1 except the holes are recessed and plate thickness is 0.25".	4-12
4	A-1/2-4R	Aluminum	Same as above with plate thickness 0.5 inch.	4-12
5	A-1-4R	Aluminum	Same as above with plate thickness 1.0 inch.	4-12
6	A-2-4R	Aluminum	Same as above with plate thickness 2.0 inch.	4-12
7	A-3-4R	Aluminum	Same as above with plate thickness 3.0 inch.	4-12
8	ZK60-5-0025	Magnesium	0.25"-diameter flaw in a 1.0"-thick test specimen located at the center.	4-13
9	M-1-X	Magnesium	Cross mark made of Dow Corning RTV 721 rubber at the back surface of a 1.0" thick test specimen.	4-14
10	S-1-1/2-W	Steel	Welded steel plate with a hole of 0.1" diameter plate thickness is 1.5".	4-15
11	A-2-1/4-00	Aluminum	Two aluminum round parts 2" and 0.25" thick, cemented with Eastman 910.	4-16
12	A-3-1/2-4R	Aluminum	Three aluminum parts cemented with Eastman 910. Solid parts are outside while the middle part is a part No. A-1/2-4T.	4-11

reflection. This is seen in Figure 4.8a as bright spots within the dark flaw images. When the holes are plugged with ρC rubber, the bright spots disappear (Figure 4.8b). It is apparent from Figures 4.7 and 4.8 that the images obtained in the reflection mode through the membrane are essentially of the same quality as those obtained in the immersion-reflection mode.

Figure 4.9 shows the image of the flaws of part No. A-1/2-4TA at 36 MHz, which was the highest frequency at which the flaw image was recognizable. Note that these tests were conducted employing the two Electronic Navigation Industries Models 350-L operated in parallel and delivering power on the order of 100 watts peak.

The next test was conducted on a 3-inch long test specimen, part No. 4-3-4R. The photographs of the flaws are shown in Figure 4.10 at three different frequencies. The flaw image is quite faint at 15.3 MHz apparently due to high acoustic power absorption. The resolution of the image is poor at 8.4 MHz.

Another test specimen (part No. A-3-1/2-4R) was tested employing the same setup but at different frequencies (see Figure 4.11). It was apparent that as the frequency was increased from 8.4 MHz the first bonding interface started reflecting a significant portion of the acoustic power. Almost all the acoustic power was reflected by the bonding interface at 20 MHz.

It was apparent from these test results that higher electrical power was needed to obtain clearer flaw images. The remaining tests were conducted employing a transducer amplifier of 200 watts peak power capability (Arenberg Model VI, see Section 3.0).

Figure 4.12 shows photographs of the flaws of test specimens of thickness ranging from 0.25" to 3.0". The flaw image obtained with higher acoustic power appears to be brighter and clearer. The test results, specifically for thicker test specimens, indicate that optical alignment is a crtical factor to obtain undistorted flaw images. As expected, the resolution of the images of 0.25" and 0.5" thick test specimens is better than that of 3" thick test specimens.

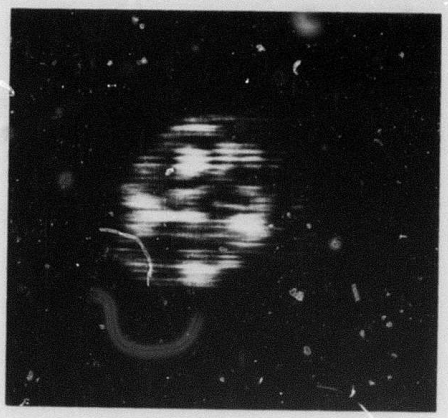

(a) Acoustic frequency: 8.4 MHz

(b) 12 MHz

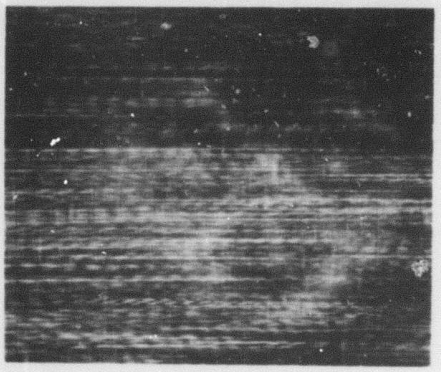

(c) 15.3 MHz

Figure 4.10: Images of the flaws of part No. A-3-4R at different frequencies. Nonimmersion pulse-echo mode of operation.

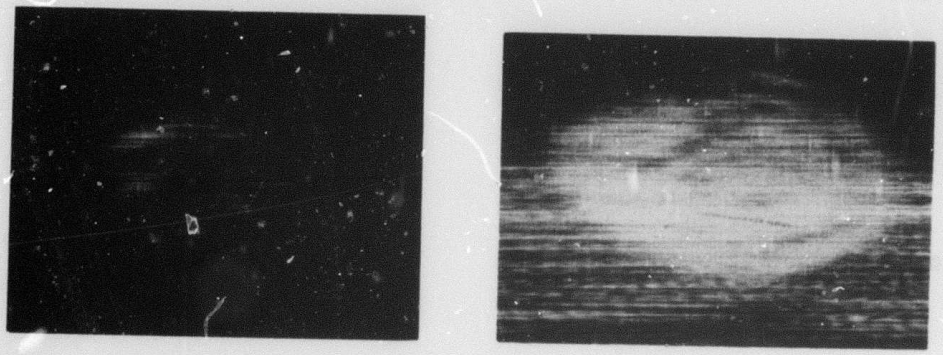

(a) 12 MHz

(b) 15 MHz

Figure 4.11: Images of the test specimen part No. A-3-1/2-4R in a nonimmersion pulse-echo mode of operation. No flaws were visible at 19.5 MHz frequency.

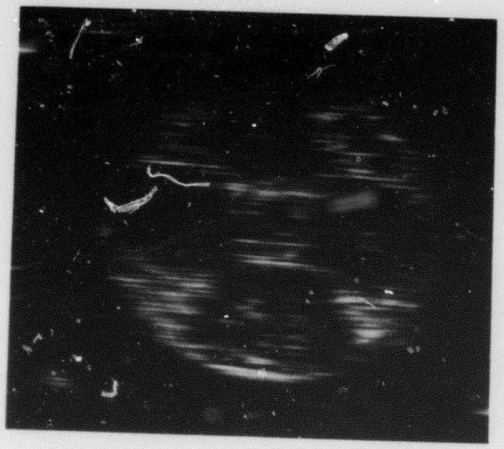

(a) Part No. A-1-4R

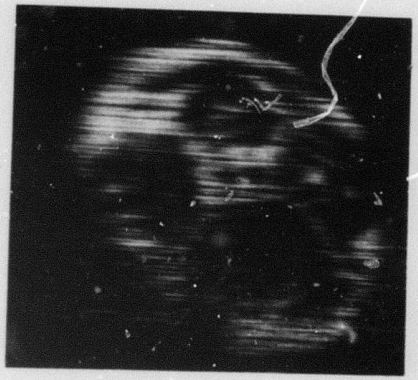

(b) 3" thick test specimen
Part No. A-3-4R

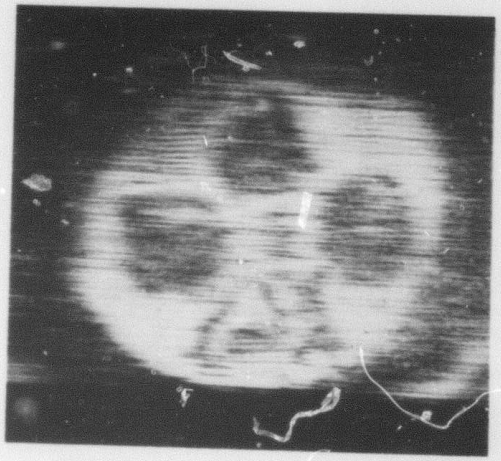

(c) 0.25" thick test specimen
Part No. A-1/4-4R

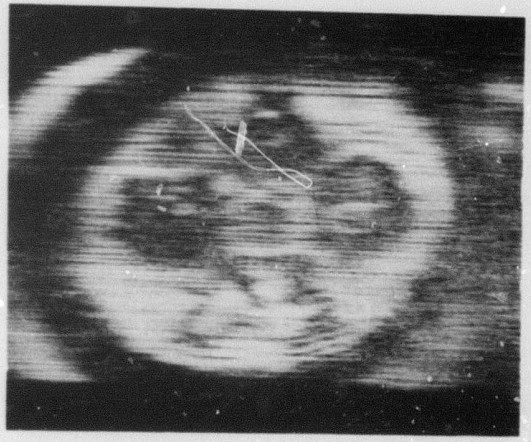

(d) 0.5" thick test specimen
Part No. A-1/2-4R

Figure 4.12: Images of the test specimens of thickness ranges from 0.25" to 3" at acoustic frequency of 18.7 MHz in a nonimmersion pulse-echo mode of operation.

The remaining test specimens described in Table 4.3 were tested and their flaw images are given in Figures 4.13 to 4.16.

The 5" x 5" transducer array, consisting of four x-cut quartz plates, was also tried. The image of the plate in the transmission mode with a "T" shaped object (Figure 4.3) is shown in Figure 4.17. Flaw images made with this transducer were not as clear as those obtained using the 2.5" x 2.5" transducer because of the decreased acoustic intensity.

4.4 Test Results Analysis

The test results indicate that the nonimmersion pulse-echo AOI system can be employed to image flaws in a solid test specimen and to find the bond characteristics of bonded test specimens.

The test results also indicated that images of flaws very close to the front surface were somewhat masked by the reflection of the front surface of the test specimen. The image of the flaws of test specimen part No. A-1/4-4R indicated that the flaw 1/8" deep can be imaged with relative ease. In addition, as shown in the videotape, a flaw only 0.03" deep from the front surface in a 0.06" thick aluminum plate was also imaged. This test result indicates that the system has a flaw depth resolution of at least 0.03". The delay time stability and resolution of the system is on the order of 0.2 microsecond. This will introduce the flaw depth ambiguity in aluminum on the order of 0.022 inch. Therefore, to increase the flaw depth resolution, better delay time stability and wider transducer bandwidth are required. The requirement of the acoustic transducer bandwidth can be explained as follows (Figure 4.18). For a test specimen consisting of aluminum, 70% of the power is reflected and 30% of the power transmitted through the water-aluminum interface. Out of 30% of the power, only 9% of the original power is transmitted through the aluminum-water interface (Section 1.0). The delay time τ of the flaw reflected sound pulse from the front surface reflection is given by the following expression

$$\tau = \frac{\text{flaw depth} \times 2}{\text{velocity of sound in the test specimen}}$$

For example, if the flaw is 1/8" deep in an aluminum test specimen, τ is on the order of one microsecond.

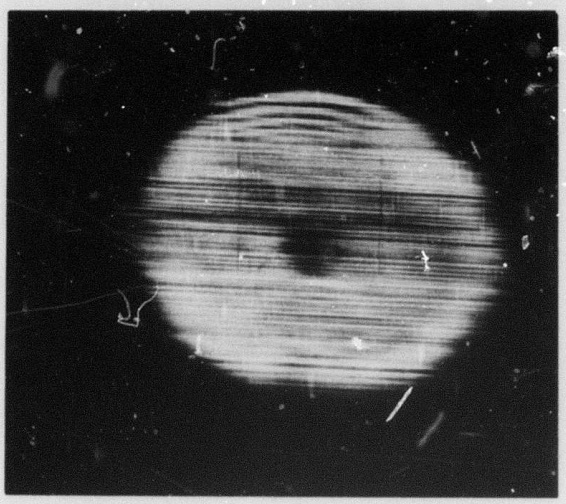

Figure 4.13: Image of the flaw in a test specimen part No. ZK60-5-0025. Acoustic frequency: 18.7 MHz. Nonimmersion pulse-echo mode of operation.

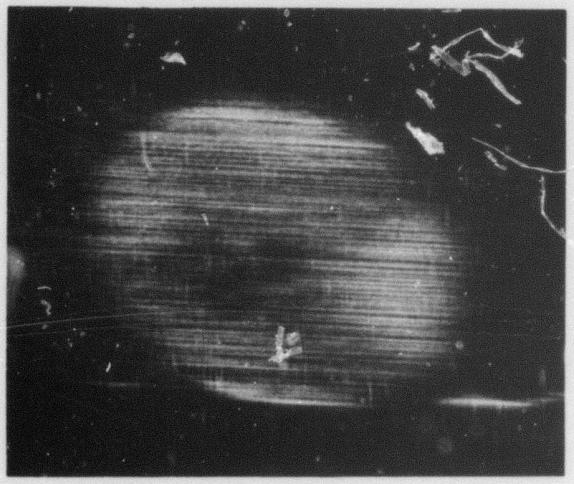

Figure 4.14: Image of the cross made of Dow-Corning RTV 721 at the back of the test specimen part No. M-1-X. Acoustic frequency: 18.7 MHz. Nonimmersion pulse-echo mode of operation.

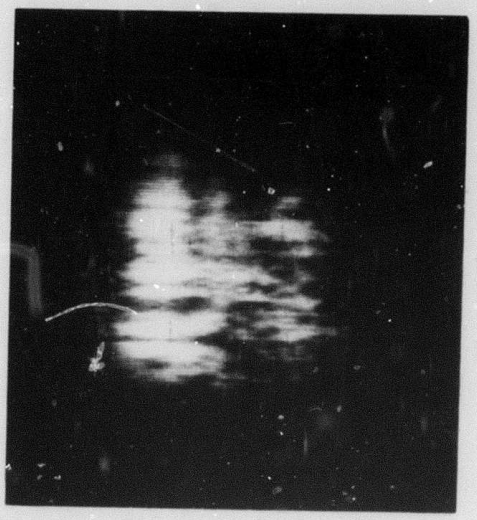

Figure 4.15: Image of the hole in a welded steel plate part No. S-1-1/2-W. Acoustic frequency: 18.7 MHz. Nonimmersion pulse-echo mode of operation.

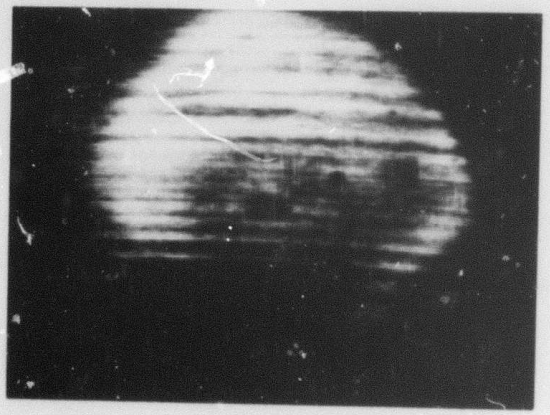

Figure 4.16: Image of the bonded aluminum parts with Eastman 910 part No. A-2-1/4-00. Acoustic frequency: 18.7 MHz. Nonimmersion pulse-echo mode of operation.

Figure 4.17: Image of a 5" x 5" transducer array with a T in a transmission mode.

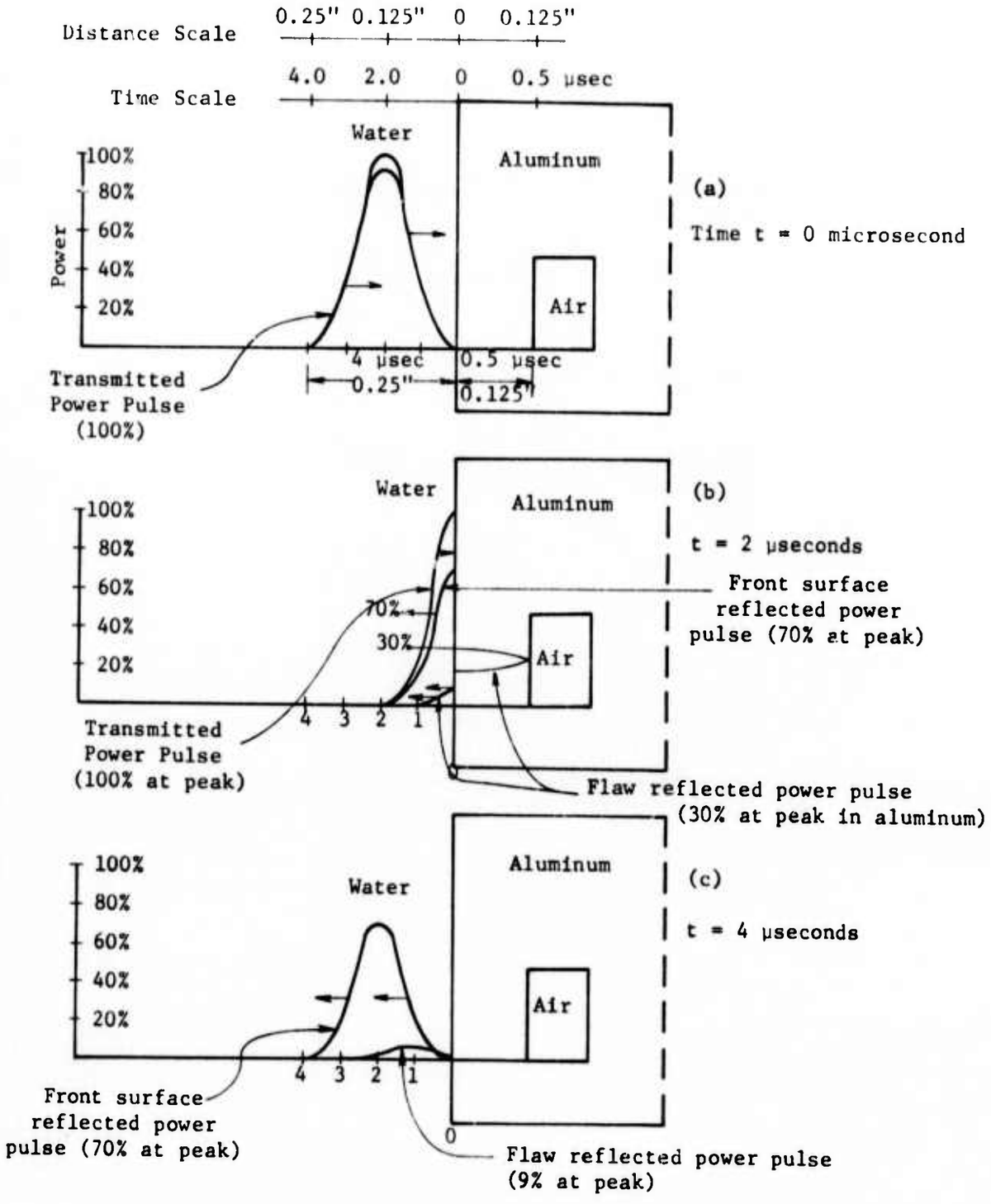

Assumptions: Pulse travel time in water ≈ 16 microseconds per inch
Pulse travel time in aluminum ≈ 4 microseconds per inch

Figure 4.18: The acoustic power before and after reflection from the flaw.

The minimum pulse width, which is limited by the bandwidth of a castor-oil backed transducer is 2.7 μsec (for a bandwidth of 370 KHz). As shown in Figure 4.18c, to obtain an image of the flaw in this case becomes quite difficult. The situation would be even more difficult for test specimens consisting of steel having much less flaw reflected sound power. Therefore, a possible solution to this problem is to increase the bandwidth of the transducer and operate at higher transducer power. Higher transducer power is required since for a constant applied transducer voltage, increasing the bandwidth decreases the acoustic power density.

The resolution of the image, as discussed in Section 1.0, is a direct function of acoustic wavelength. For greater resolution, the acoustic frequency must be increased. As shown on the videotape, the smallest diameter hole imaged in a nonimmersion pulse-echo mode is 0.03 inch at 15 MHz acoustic frequency. The analysis predicted that the area resolution at 15 MHz is on the order of 0.02 inch.

5.0 CONCLUSION AND RECOMMENDATION

The primary objective of this project was to design and develop a workable nonimmersion pulse-echo imaging system and to demonstrate that the images of flaws within the test objects can be obtained without immersing the object in the liquid and requiring access to only one side of the object. The secondary objective was to identify and incorporate the improvements that can enhance the system performance and determine the area and depth resolution of the flaws.

These objectives were achieved. Results obtained show that our experimental setup had a detectable flaw depth up to 3-1/2 inches in aluminum with an acoustic power of 200 watts at 15.3 MHz. Depth resolution was measured to be 1/8 inch under the same conditions. Images were obtained conveniently which had the quality implied by the following lateral resolution figures:

Acoustic Frequency	Lateral Resolution
5 MHz	.12 inch
10	.06
20	.03

Advantages of this system can be summarized as follows:

- o Does not require mechanical stability and can be utilized in a production type environment.
- o Ability to produce visual images of the interior of optically opaque bodies.
- o Operates in real time.
- o Eliminates the need for highly trained operators (because optical images are obtained and data interpretation is not required).
- o Operates in both transmission and pulse-echo sound modes.
- o Operates without immersion of the component.
- o Can provide permanent videotape record of inspection.

- Unlike many ultrasonic flaw detection techniques, there is no flaw ambiguity because of the acoustic near-field effect (Section 1.0).

Applications of the nonimmersion pulse-echo system are listed below:

- Detection and imaging of flaws and appendages in assembled structures.
- Detection and imaging of inhomogeneities due to air bubbles, boundaries and foreign materials.
- Determination of bond characteristics of laminated composites.
- Determination of real surface contact area and view of it in aerospace components such as metal-to-metal contact valves.

A videotape recording is provided containing the following items:

- Brief description of the nonimmersion pulse-echo imaging system.
- Basic principle of operation of the system.
- Advantages and applications of the system.
- Demonstration of use of the system to image and record the flaws.
- Flaw images of the test specimens having known flaws.

The R&D work associated with nonimmersion pulse-echo acousto-optical imaging system has been essentially completed. This system is ready to be packaged for use in production-type environments for quality control and assurance applications. Its applicability depends upon the nature of the part and the material to be inspected. A packaged prototype model is shown schematically in Figure 5.1.

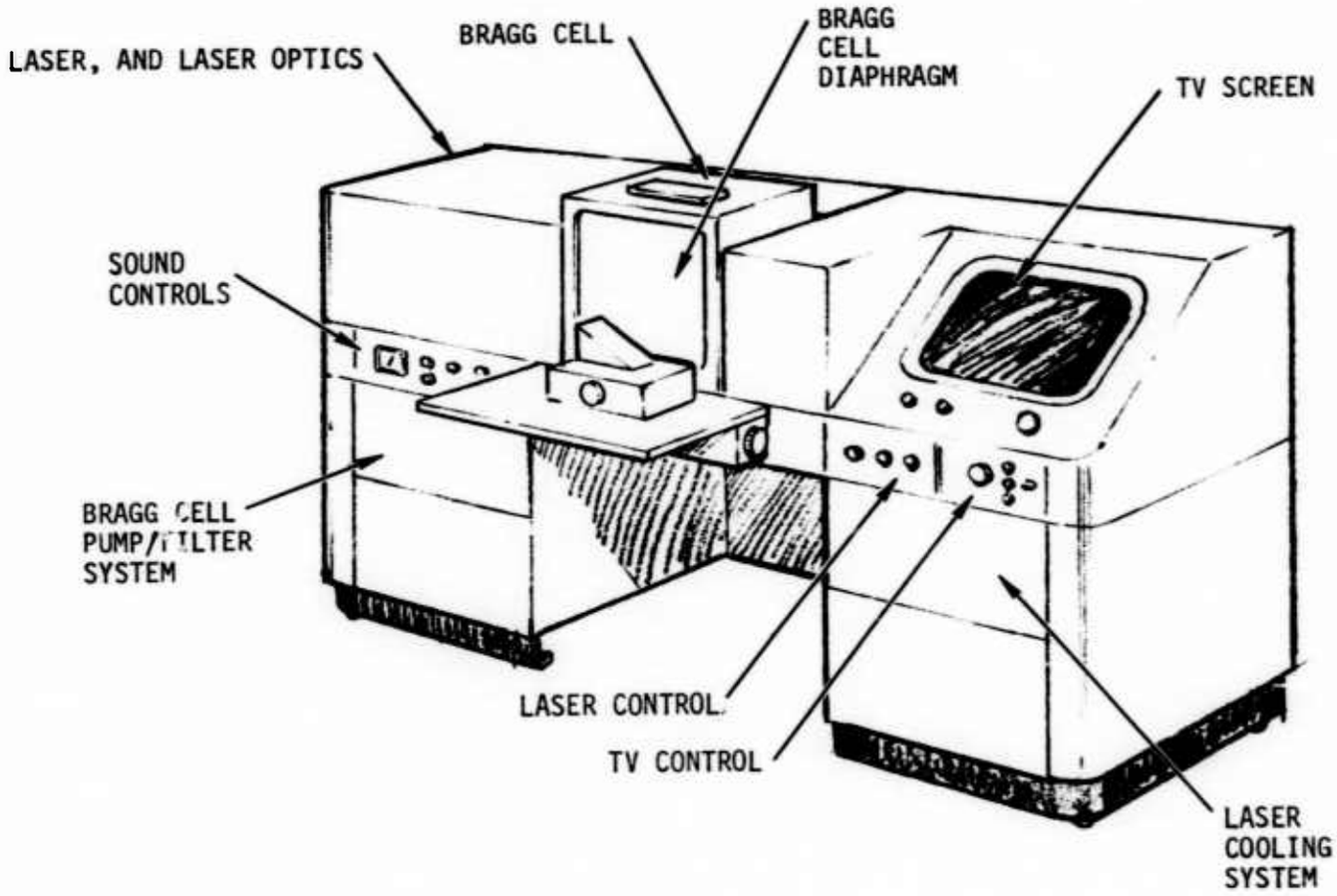

Figure 5.1: Acousto-optical nondestructive testing system.

6.0 REFERENCES

1. "Nondestructive Testing by Acousto-Optical Imaging," R. Aprahamian and P. G. Bhuta, Materials Evaluation, May 1971.

2. "Nondestructive Testing Using TRW Acousto-Optical Imaging System," R. Aprahamian, J. L. Jacoby, and P. G. Bhuta, TRW Systems Group, Redondo Beach, California. Semi-annual report prepared for Army Materials & Mechanics Research Center, Watertown, Mass. 02172, August 1971.

3. "Nondestructive Testing Using TRW Acousto-Optical Imaging System," R. Aprahamian, J. L. Jacoby, and P. G. Bhuta, TRW Systems Group, Redondo Beach, California. Interim Report prepared for Army Materials & Mechanics Research Center, Watertown, Mass. 02172, January 1972.

4. Acoustical Holography, Vol. III, A. F. Metherell, Editor, "Noise Characteristics of Bragg Imaging" by R. A. Smith and G. Wade, Plenum Press, 1971.

5. "Studies of Resolutions in a Bragg Imaging System," R. A. Smith, G. Wade, et al, Journal of the Acoustical Society of America, Vol. 59, No. 3, pp. 1062-1068, March 1971.

6. Ultrasonic Testing of Materials, J. Krautkramer and H. Krautkramer, Springer-Verlag, 1969.

7. Sonics, T. Hueter and R. H. Bolt, John Wiley & Sons, 1955.